Master thesis and internship[BR]- Master's thesis : Finite element modeling methodology of a tungsten inert gas weld on S355MC Steel[BR]- Integration Internship : CRM Group

Auteur : Sandront, Augustin
Promoteur(s) : Ponthot, Jean-Philippe
Faculté : Faculté des Sciences appliquées
Diplôme : Master en ingénieur civil en aérospatiale, à finalité spécialisée en "aerospace engineering"
Année académique : 2022-2023
URI/URL : http://hdl.handle.net/2268.2/17947

Finite element modeling methodology of a tungsten inert gas weld on S355MC Steel

University of Liège - School of Engineering and Computer Science

Master's thesis completed in order to obtain the degree of Master of Science in aerospace Engineering

Author: Sandront Augustin

Student number : S181107

Academic year 2022-2023

Supervisor: Ponthot. J-P.

Internship supervisor : Senart T.

Additional Jury Member: Béchet E.

CRM asbl

Center of Research for Metallurgy

Siège Social | Rue Ravenstein 4 | 1000 Bruxelles | Belgium • Centre Administratif | Avenue Bois Saint-Jean 21 | 4000 Liège | Belgium

TVA: BE 0406.015.373

Technical report

xxxxxxxxxx

Finite element modeling methodology of a tungsten inert gas weld on S355MC Steel

Customer :	**xxxxxxxxxx** [xxx@xxx.xxx], *xxxxxxxxx title* **xxxxxxxxxx** [xxx@xxx.xxx], *xxxxxxxxx title*
From :	xxx XXX [xxxxx@crmgroup.be], xxx XXX [xxxxx@crmgroup.be]
Reviewed by :	xxx XXX [xxxxx@crmgroup.be]
Update of the document :	xx.xx.20xx
Customer reference code :	XXX / PO # xxxxxxxxxxxxxxx
CRM Group reference code :	CRM / xxxxxxxxxxxxxxx

Xxxxxxxxxxxxxxxxxxx

xxxxxxxxxxxxxxxxxxx.

Confidentiality	xxxxxxxxxxxxxxx

CRM asbl

Center of Research for Metallurgy

Siège Social | Rue Ravenstein 4 | 1000 Bruxelles | Belgium • Centre Administratif | Avenue Bois Saint-Jean 21 | 4000 Liège | Belgium

TVA: BE 0406.015.373

Important note:SSSS

Care has been taken to ensure that the information in this publication is accurate, but this information is not contractual. The use of any information enclosed in such presentation is entirely at the risk of the user.

Under no circumstances CRM Group shall be liable for any costs, losses, expenses, or damages (whether direct or indirect, consequential, special, economic or financial, including any losses of profit) whatsoever that may be implied by the use or reference of any of the information contained in this document.

Copyright

Table of Contents

Table of figures

Table of abbreviations

FEM : Finite Element Method

LVDT: Linear Variable Differential Transformer

TIG: Tungsten Inert Gaz

HAZ: Heat Affected Zone

DOF: Degree Of Freedom

1 Abstract

Welding is a widely used fastening process, but is nevertheless extremely complex. The merging of a non-conventional heat input and a complex material compose a multi-layered problem that has been studied since the XIX century. In this manuscript, a Tungsten Inert Gaz weld on S355MG steel has been investigated and reproduced using the LS-Dyna Software. This work lays the foundation for further research on the welding phenomenon so that, eventually, the residual stresses and deformation induced by the fastening of two steel parts can be predicted with a sufficient level of confidence.

To this end, an experimental setup was developed, with the aim of reproducing it with a Finite element software. Two main variables of the problem were measured: the temperature and the displacement. Two separate experiments were necessary to retrieve this data, who was then compared to the output of the Finite Element model.

Temperature similarity was reached for the data set of the first experiment by neglecting the convection. Applying the same adjustments to the parameters given by the second experiment did not induce temperature similarity however. The displacement of the plates were not reproduced as well. The neglection of convection has thus to be discarded and leads on new parameter adaptation are explored.

2 Introduction

The CRMGroup company, which is specialized in metallurgy research, was developing a steel floor to be used in the industry (Figure 2-a). A major issue was discovered during the welding process of the beforementioned component : a large residual deformation was induced, which caused the floor to be unsatisfactory to be released as can be seen on Figure 2-b. To understand this phenomenon, the company reached to the University of Liège for a student to perform his master thesis on the welding process, and more specifically on its modeling. The thesis is the one present in your hands at the moment.

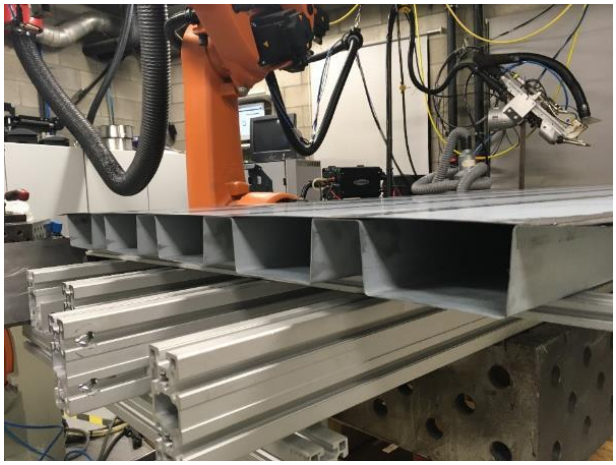

Figure 2-a : Steel floor developed by the CRMGroup company before welding

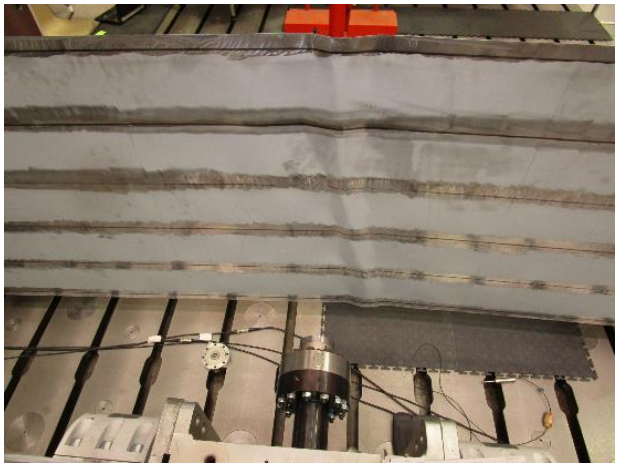

Figure 2-b: Steel floor developed by the CRMGroup company after welding

The objective of this manuscript is to initiate a methodology that will ultimately guide further studies in their analysis of different welding processes, applied to different configurations. For clarity, the methodology will be here synthesized thanks to a bullet list, but can obviously be more complex and less linear in its final form: the process might cycle through multiple steps for instance. In this manuscript, the tool development stage is to be initiated, further work will be necessary to develop the entirety of the methodology.

Here is the methodology's, and by extensions this manuscript's, structure.

1. State-of-the-art analysis
2. Tool definition
3. Tool development
4. Influence of tool parameter modification
5. Tendency reproducibility in experimental setup
6. Implementation of the tool in another model and behaviour analysis

The state-of-the-art part is simply documentation analysis, as to not reproduce previously done work and learn the basis of welding reproduction in FEM. The tool definition states the welding process studied, the material used, the software and more parameters that characterize the study. In the present manuscript, all modelling has been performed using LS-Dyna Pre-post software, and the 12th version of the LS-Dyna solver. Another software, FabWeld, has been used to define the material model from exterior data [1]. The Fabweld software uses the LS-Dyna nomenclature to prepare welding models. It was used for the first iterations of the model, but was discarded later as too many unnecessary parameters were defined, only the material definition was kept.

Finally, the tool development part is the heaviest one, which consists in model and experiment development, and result correlation. Item 4 and 5 will allow the model to have defined boundaries: a maximum welding speed, a minimum sheet thickness, and so on. As stated previously, these stages are not discussed in the present work.

3 State of the art

The study of the mechanical effects of the fusion welding processes by finite element method started in the early 1970s. In 1980, Masubuchi in [2] stated :"Hopefully, it will only be a short time before the computer simulation of simple joints such as the fabrication of a built-up beam and the one-pass welding of a butt weld becomes commonplace industrial practice". Even if he later came back on this statement, it is nowadays a reachable goal. Indeed, in 2022, it was proven that thermal elastic-plastic finite element analysis can help improving crack resistance in larger structures, as well as improve the welding efficiency and reduce its cost [3]. In between those two dates, a great amount of work has been done on the two major axes that welding process modeling implies: the heat distribution definition and the material model. The two beforementioned points will be addressed in the following sections.

It is important to note that the uncertainty on both the heat input and the material properties have as consequence that modeling of the welding phenomenon depends strongly on the experimental results: the model parameters have to be adjusted to reach similarity with the experiment. This problem, added to the fact that welding processes are notoriously hard to model due to the large amount of nonlinearities present [4], is one of the reasons why welding is not yet implemented in every model of larger structures

3.1 Tungsten Inert Gaz welding

The fusing welding process is defined as a technique to join materials, using heat to melt them together. Once the material has cooled down, the fused materials have some resistance to separation. The welding process can be done on a lot of materials, but the one of interest here is steel, as this was the metal used in the floor presented in the introduction. The method with which the heat is brought has a great importance: laser, friction, ultrasound, and electric arc are a few of them. Each of these methods can then be subdivided into more precise methods. For the sake of simplicity, only one method will be addressed here, a method which uses an electrical arc: the Tungsten Inert Gaz method (TIG). One should, however, know that certain other fusion welding processes are modelled similarly, the work done in this paper on the TIG process could be reproduced on the laser or electron beam methods for instance, with a modification of the weld pool definition [5] & [6] .

In TIG, the heat is produced by a non-consumable tungsten electrode and the material that is to be welded [7]. The molten material (called weld pool) as well as the heated one has a

tendency to oxidize very quicky, which is why an inert gas is blown on the weld location. Figure 3-a is a schematic of the process.

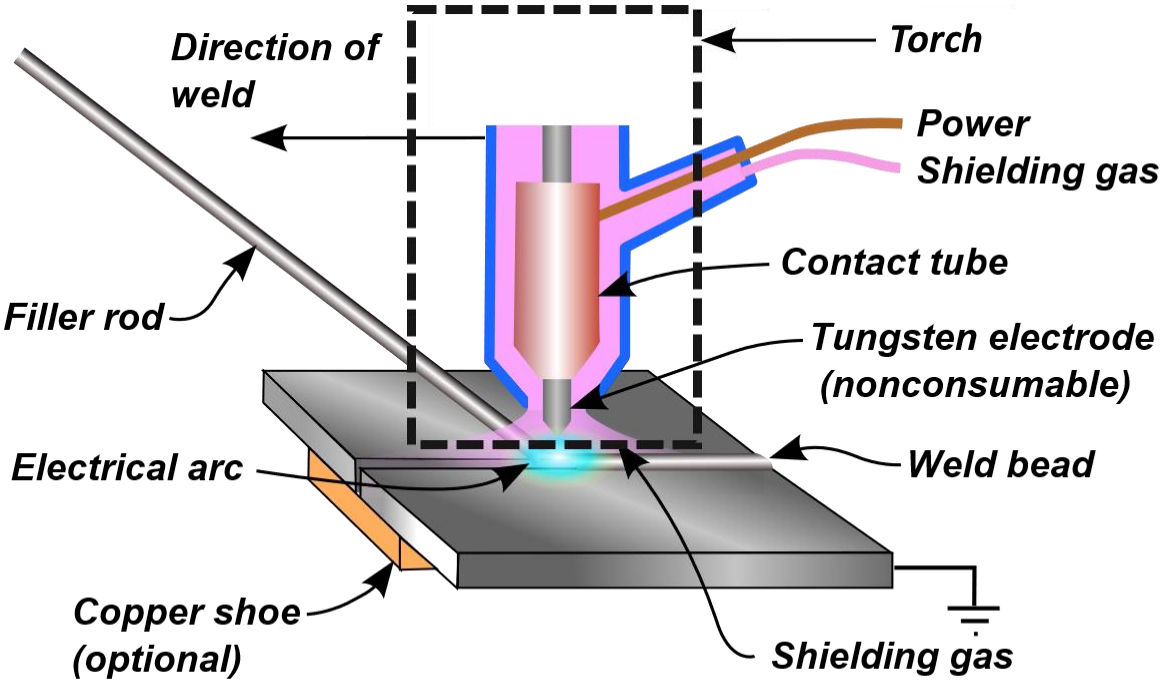

Figure 3-a: Schematic of the TIG welding process [8]

The TIG method has considerable advantages, which enticed its choice for the present case. First and foremost: TIG welding is and will remain an important process in the industry, due to its equilibrium between precision and polyvalence [7]. Indeed, TIG welding is very precise due to the concentrated heat input of the electrode. Laser welding is of a greater accuracy still, however, it cannot be performed by hand, and thus is hardly possible for on-site problems. Moreover, TIG welding can be executed on a large panel of materials, with or without filler material and can be automatized easily. All perks that will come in handful when designing the experimental setup. Finally, the parameters of a TIG weld have each a characteristic influence on the final result and are mostly independent from each other [7]. This last aspect is very useful when adjusting the model to the experimental results.

Now that the concept of TIG welding has been defined, the reader should understand the interactions that the welding process has over the material. These interactions can be defined by a communication between the thermal and mechanical states of the system. They are depicted on Figure 3-b and Table 1 [4]. The first schematic represents the couplings that

are present between the three physical fields : the heat flow, the deformation and the microstructure.

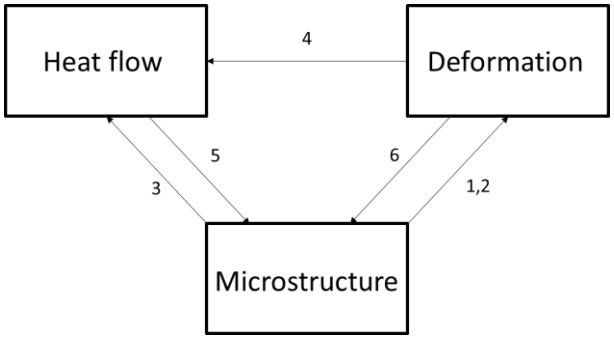

Figure 3-b: Schematic of the interactions between the different fields during a welding process [4]

Coupling number	**Description**
1a	Thermal expansion depends on the microstructure of material.
1b	Volume changes due to phase changes.
2a	Plastic material behavior depends on the microstructure of material.
2b	Elastic material behavior depends on the microstructure of material.
3a	Heat conductivity and heat capacity depend on the microstructure of material.
3b	Latent heats due to phase changes.
4a	Deformation changes thermal boundary conditions.
4b	Heat due to plastic dissipation (plastic strain rate).
4c	Heat due to thermal strain rate.
4d	Heat due to elastic strain rate.
5	Microstructure evolution depends on temperature.
6	Microstructure evolution depends on deformation.

Table 1: Different thermo-Mechanical couplings present in welding [4]

Couplings **4C** and **4D** can be neglected due to the importance of the heat input of the welding process itself (and the fact that **4D** is included by the modification of the heat capacity of the material) [4]. Coupling **4B** can be neglected as well [4]. It is, however, a behavior taken into account in the LS-Dyna Solver [9].

These interactions between three fields of knowledge is one of the major obstacles that weld process modelers had to overcome. In most cases, the microstructural field is not modelled per se, but replaced by experimental data of the parameters of the material at different temperatures. And the information is thus mostly exchanged between the thermal and mechanical fields, as will be demonstrated by the use of a coupled thermo-mechanical solver.

3.2 Heat pool modelling

In 1985, John Goldack presented an hypothesis on the shape of the heat pool for arc fusion welding and proved that it gave accurate results [10]. The shape is a double ellipse, in the direction of the weld and in the direction of the torch. On this volume, the heat power is distributed in a bell-like shape, with the peak coinciding with the torch emplacement. The exact equation of the distribution can be seen in [11]. On Figure 3-c, the X-variable is the weld direction, and the welding torch coincides with the Z-axis.

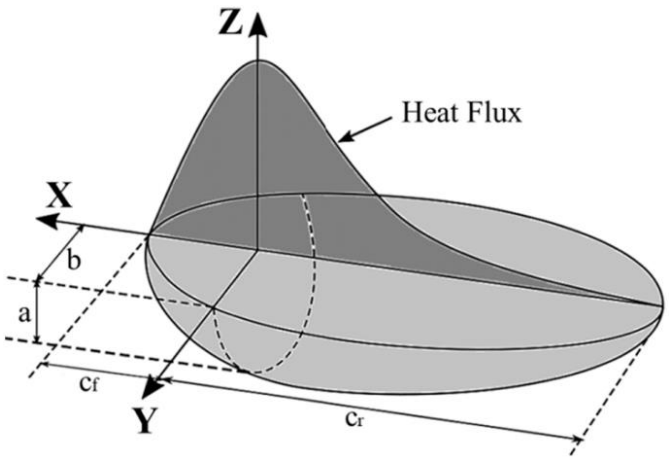

Figure 3-c : Goldack model for the heat input of an arc welding process in finite element method [11]

Much later, it was specified that this distribution of the heat is actually not perfectly accurate, and that a constant distribution is sufficient and closer to reality [12]. A representation of the distribution can be seen in Figure 3-d . That will be the model chosen in this paper. As can be seen in Figure 3-d, the heat distribution is not equal in the front (denoted by **f**) side of the ellipse and on the rear (**r**) side. It is a convention that the front part contains 60% of the total heat energy and the rear part 40% [13].

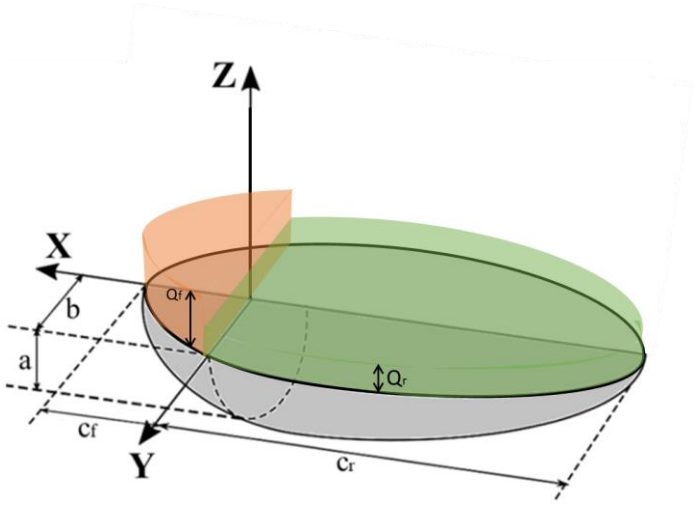

Figure 3-d: Modified Goldack model for the heat input of an arc welding process in finite element method [11]

In practice, this double-ellipse shape has to be similar to the weld pool of the process, which is, by definition, the region where the material reached the liquid state at one point in the process. The dimensions of this weld pool will be identified thanks to a metallography. Metallography is the process of extracting cutoff of the welded material, polished and cleaned it so that the heat affected zone could be seen.

3.3 Material properties of steel

The material chosen to be welded here is the S355 MC steel, due to its availability, well-furnished property data set and relevance as it was used to create the steel floor presented in the introduction. The reader is not without knowing that steel is a rather hard material that has a specific behaviour to temperature. Indeed, the higher the temperature, the lower the yield stress, the Young modulus, and most importantly the lower the density.

Not only the temperature, but also its rate of change has importance: the speed at which the steels cools down changes the microstructure of the cold material. This has obviously a great importance in the welding field, as once the process is done, the steel that has melted may not have the same microstructure as the remaining part of the component that was not heated as much. Materials with different properties will then coexist in the welded part, that will in consequence behave differently that one of a unique homogeneous material: modified crack resistance, residual stresses, corrosion behaviour, etc.

Steel is composed of five phases that differ from one another with crystalline structure: ferrite, martensite, austenite, perlite and bainite. Those five phases, with different material properties, are primordial to acknowledge. To assess the composition of the steel, a CCT steel graph can be used, as the one that can be seen in Figure 3-e. A high cooling rate induces the production of martensite. Then, lowering this cooling rate, bainite, ferrite and pearlite will appear.

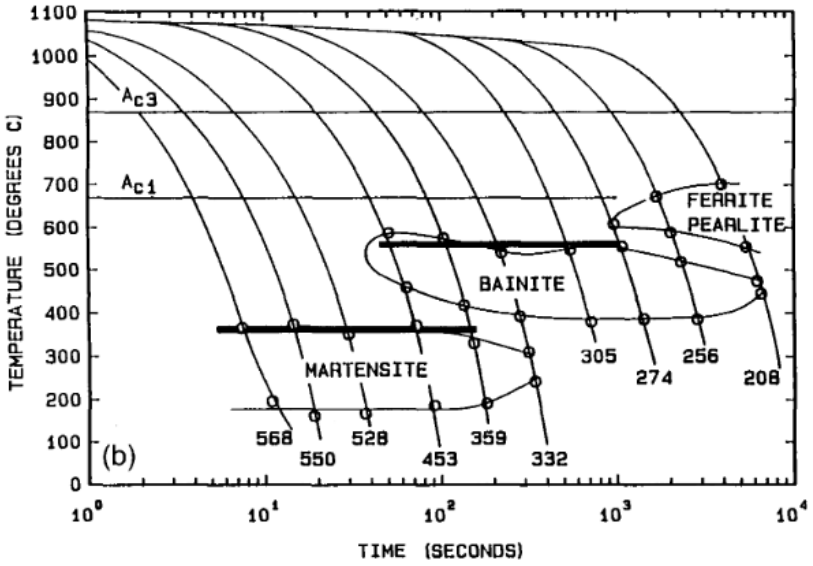

Figure 3-e: Typical CCT graph of Steel [14]

The process of welding consists of a highly concentrated, precise heat input to a specific location of a component. The material right beneath the torch undergoes high temperatures, but further from the weld line, there exists matter that does not change its microstructure at all due to the temperature rising to a lower value. The boundary between the material whose properties have been changed by the welding process and the material who has not marks the end of the Heat Affected Zone (HAZ). The HAZ is thus the region where the material changed due to temperature, and the modification of the properties of the whole component are due to the material contained in this zone. An example of HAZ can be seen in Figure 3-f, which is a cutoff of an experiment performed in the scope of this manuscript, a metallography. On the right of the weld, the heat affected zone is highlighted with a dashed line. On the other side of the weld, the HAZ is not marked with a dashed line, so that the reader could notice the shade change between the inside and outside of said zone. The black material in which the sample sits is resin, and the red lines are generated by the microscope and are not to be considered here.

As the phase (and thus material) is modified, the hardening curve differs from place to place in the material. The hardening curve dictates the behavior of the deformation once the plasticity is reached, thus whenever the deformation is no longer reversible (or “elastic”). All of the data necessary for the modeling of such a material is found in [1] and is assembled in LS-Dyna via the FabWeld Software as explained previously.

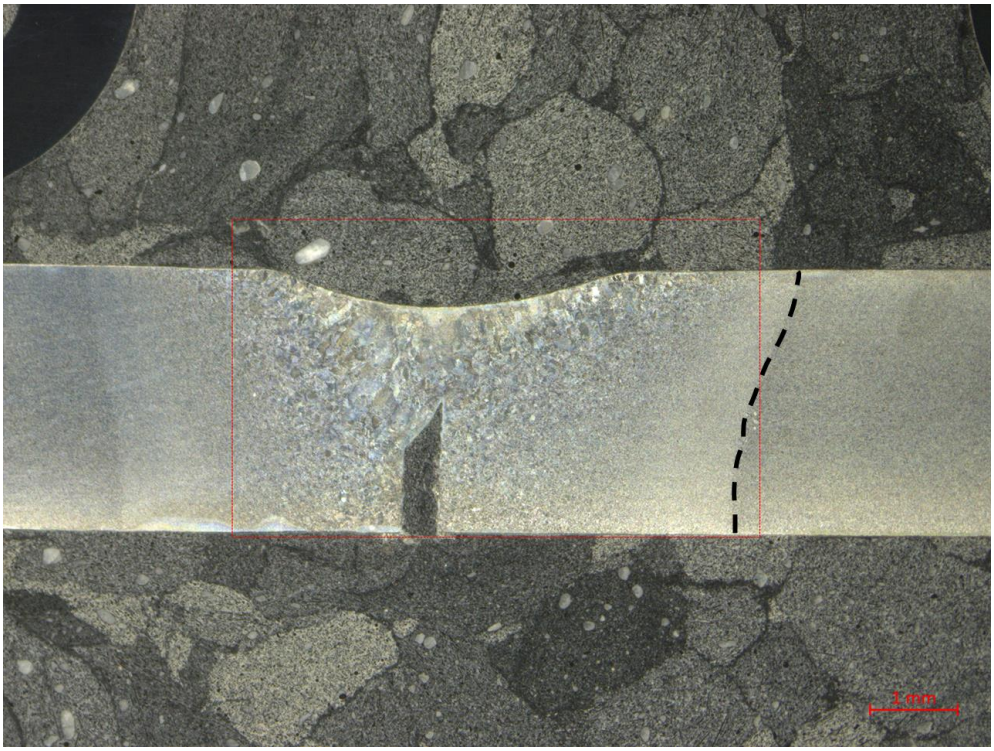

Figure 3-f: Metallography of a sample done for this manuscript, with the HAZ highlighted by the black dashed line

3.4 Material model

Steel, as explained in the previous section, is a well-studied material with a lot of data available. However, its internal properties vary greatly with temperature. At high temperatures, data retrieving experiments such as tensile tests are far from effortless and material properties are thus lesser known. This is why, historically, a cut-off temperature was set: by a certain point in the heating process of the model, the material properties would not evolve with temperature anymore. The cut-off temperature has thus been used to replace unknown material data at high temperatures. It is not needed anymore, at least in this model, as the liquid state of the material is considered as an autonomous material that has its own properties.

But, as shown before, the material properties of steel do not uniquely depend on the current temperature of the material but also on the peak temperature, as well as the cooling rate applied on the material. All along history, multiple models aimed at representing the phases and properties of steel were explored but nowadays, the use of an implemented CCT diagram similar to Figure 3-e is the most common one [4].

The major computational issue that can occur while modelling a material law in the thermal solver is the latent heat associated with the phase change. Whenever steel changes from martensite to austenite for instance, a part of the energy that is at other times used to heat the material goes to the re-disposition of the atoms of the material. The amount of energy needed to perform this is called the latent heat. Various models have been studied, but the most relevant one is the effective heat capacity.

Effective heat capacity uses the heat conductivity λ and capacity *c* to include the phase change. For pure materials, as the phase change occurs, heat is absorbed (or released) by the material but its temperature does not evolve, one could assume that it has an infinite heat capacity. To avoid using an infinite artefact, a temperature range is set. For alloys such as steels, the phase change happens over a temperature range, from solidus to liquidus, there is thus no need for an artificial temperature scope. The mechanism stays however the same as the heat capacity is modified over the whole temperature range. The effective heat capacity is then computed with this temperature range and the heat input necessary to reach from one to another phase. LS-dyna uses a more direct method: the latent heat is considered as an external heat input, positive or negative, that is activated at each phase change.

3.5 Similar research

Existing studies over the FEM representation of a welding process are mostly divided in two topics: parameter optimisation and deformation/internal stress reproduction.

The parameter optimisation procedure attempts to reproduce welding processes to reach a goal in the quality of the weld : total penetration, low residual stresses, low porosity, etc [15] [16] [17].

The present manuscript is in the second topic: attempting to reproduce an experimental data set with the hope to later use the internal material data in larger structures [18] [19] [5] [20].

4 Numerical Tool

The tool developed in this paper is, as stated previously, a finite element model. This model will be then fed into the LS-Dyna solver, more specifically its twelfth version. This section will describe the assumptions made to define the model as well as the numerical parameters and the reason of their choice.

This model will then be compared to experimental results to prove its relevance. As the computational domain offers few restraints, the experimental setup will actually be the basis of the model, which is why it is exposed before the numerical model.

4.1 Experimental setup

The two major measures that will be output by the experiment will be the thermal profile and the vertical displacement of the end of the plate. Both measures were a part of the experimental process of [13], the setup is inspired by their studies.

The base of the setup is an ensemble of two plates as can be seen on Figure 4-a: one of 20X20 cm and another of 25X20 cm. The two plates are to be welded without any filler metal, on the 20-centimeter side. These dimensions were chosen with the advice of technicians as to avoid having an edge effect at the measurement point, as well as to obtain a vertical displacement to the plate sufficient of be measured. The edge effect in question here is the initiation of the weld process, as well as its termination, which could induce discrepancies from an experiment to another. Indeed, at the start of the weld line, the torch has to accelerate up to the final weld speed, which induces a different behaviour than when the weld speed is constant.

The plates are 3 millimeters thick. This thickness was chosen as TIG welding is harder to perform on thinner plates, and thicker plates would induce lesser deformation and be out of the scope of the use in the steel floor. The two plates were first spotweld together, using TIG as well and with the same parameters as the final weld process will use. The spotwelds are necessary for the plates to be able to hang in air without any interaction with other solid materials, which could absorb heat.

To avoid any heat spreading to other pieces that might be present, the clamping was chosen as can be seen in Figure 4-a, in transparent light grey. Only the excess 5 centimeters of the longer plate are clamped, the rest is floating around in air, as the two plates are already tied

with the spotwelds. This setup prevents any large heat flow to the clamp. In Figure 4-d, one can also notice the thermocouples, which are represented with red dots, the welding torch and its direction (green and yellow), as well as the Linear Variable Differential Transformer (LVDT), that is used to measure the displacement during the welding process (blue).

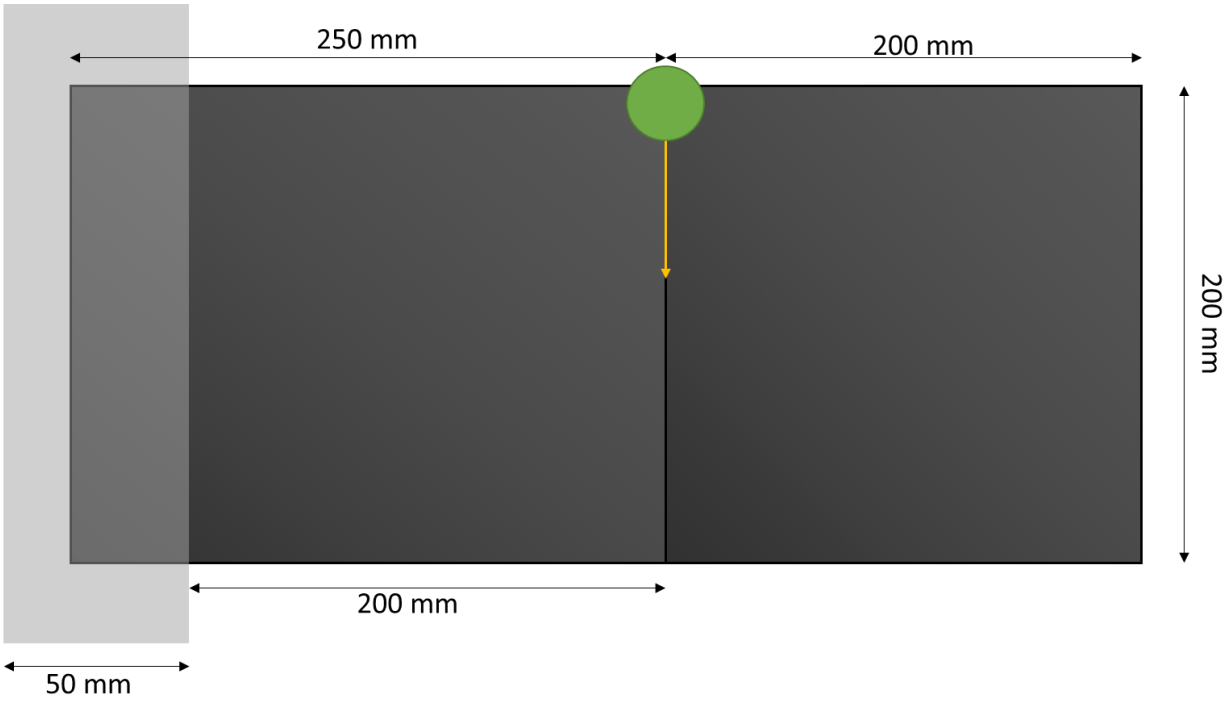

Figure 4-a: Schematic representing the experimental setup seen from the top of the plates; the weld torch is in green, the weld direction in yellow and the clamps in light gray

Thermocouples were placed at 5, 15, 25, 35 and 45 millimetres from the weld to assess the different cooling rates. They are each spaced from one another of one centimeter to prevent any interaction between them. This last precaution was taken as a recommendation from the technician. A LVDT placed at the middle point of the plate to measure the vertical displacement. It uses a voltage differential to assess the displacement of the material, per its name. This location is chosen to allow a visualization of the displacement before the torch passes the middle point, as well as when and after it does. The disposition of the sensors on the small plate can be seen in Figure 4-b: the red circles represent the thermocouples, the green circle and the arrow are the torch and the weld direction, and the blue device is the LVDT.

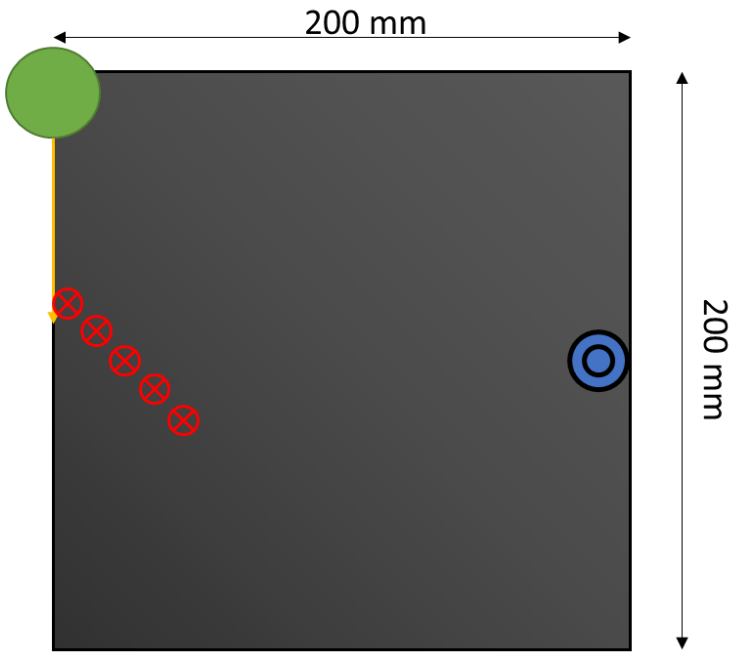

Figure 4-b: Schematic of the sensor disposition on the small plate, the thermocouples are red, the torch green, the weld direction yellow and the LVDT blue

A first batch of welds was done, where the objective was mainly to calibrate the measuring instruments and asses the correct speed and heat input. Too low of a weld speed would induce a total penetration of the weld (the material is molten in the whole thickness of the plate), which reduces the amount of distortion induced in the plate. The state of the weld can be considered bad if the weld speed is too high, in contrast. In the end, the weld speed was chosen to be 3.33 millimetre per second. The amperage and voltage has been chosen following the advice of the welding specialist in the workshop, with as objective to reach a penetration of 1.5 milimeter: it was set to 120 A and 15 V.

Once the setup was fixed, a batch of six experiments were done as to have repeatability in the data. Figure 4-c shows the experimental setup of the last plate. The first image is a side view of the experiment, where the welding torch will end after the process. The second image represents a top view of the setup and the last one places the view perpendicular to the weld. The green cables are the thermocouples, and the arm holding the LVDT is at the forefront of the rightmost image.

The whole experimental setup is depicted in Figure 4-d, with the red circles being the thermocouples, the blue device being the LVDT and the green device being the TIG weld torch.

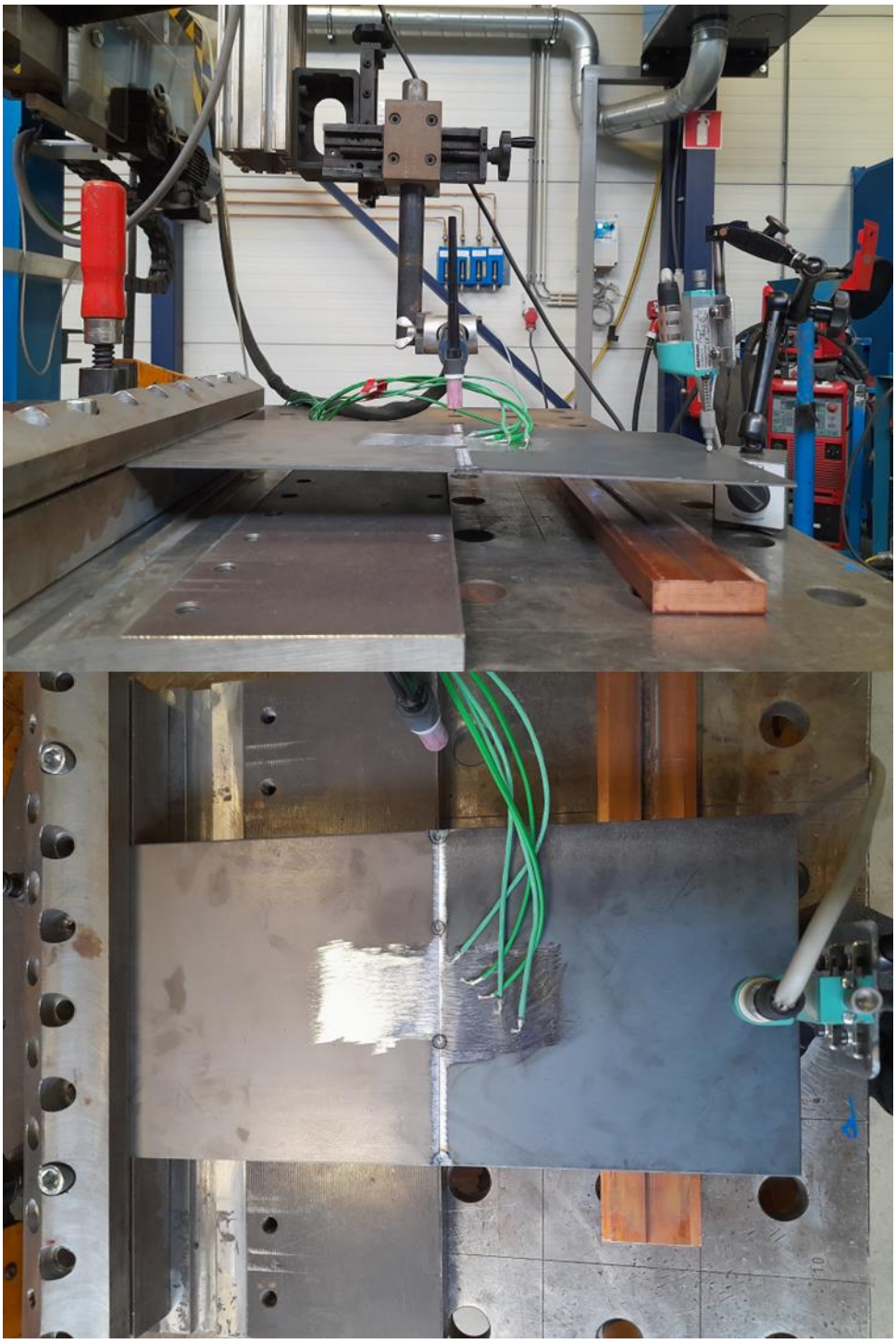

Figure 4-c: Experimental setup seen from the end-of-weld side, the top and the furthest side from the clamp with the thermocouples (green wires), LVDT (metallic part containing a spring)

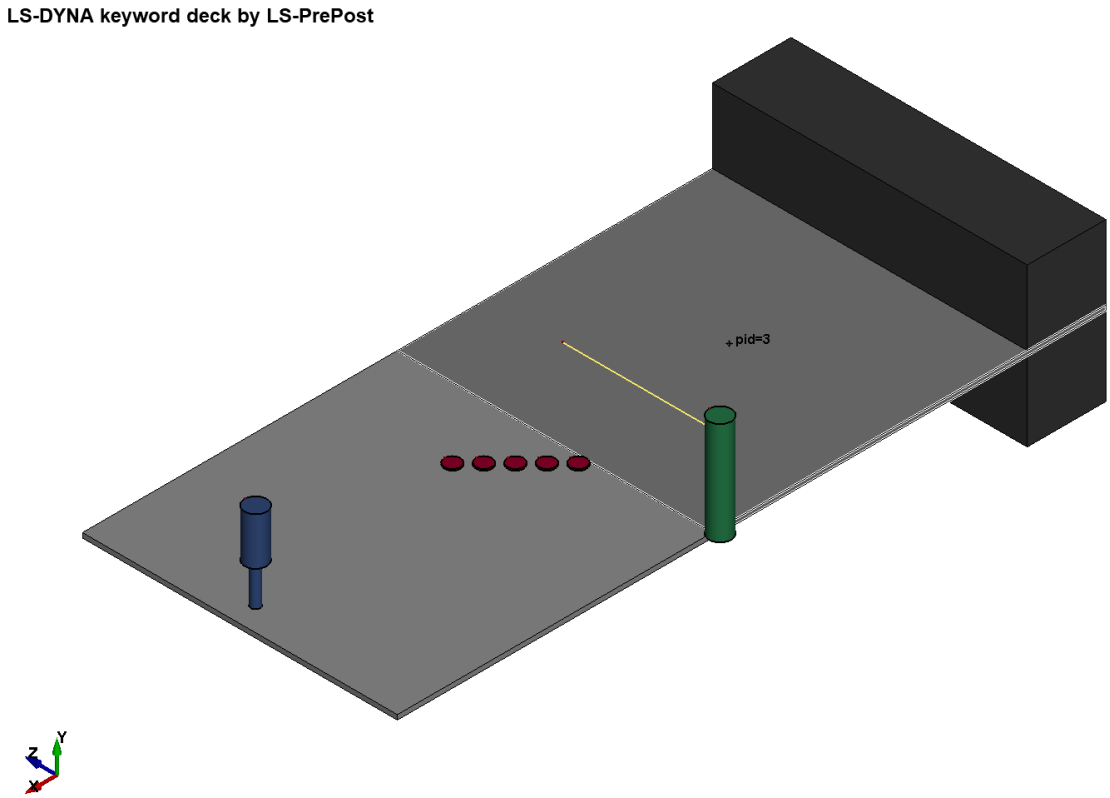

Figure 4-d: Schematical representation of the experimental setup containing the weld torch (green), the weld direction (yellow), the thermocouples (red) and the LVDT (blue).

As beforementioned, the displacement output of the first batch of experiments was not conclusive. A second batch of experiments was then performed, with four plates and a smaller heat input: 110 A and 15 V. A supplementary LVDT was used as well. Unfortunately, due to the lack of time to calibrate the instruments, a singular plate came out of this campaign wholly weld. The three other plates had to be passed twice to be welded along the whole length, which does not allow for consistent results. The one-shot welded plate will be analysed for temperature and displacement correlation. However, due to the lack of repeatability, the conclusions made on this batch of experiments are to be considered with care.

4.2 Model setup

The tangible part of the model comes directly from the experimental setup. The reader should be aware of the fact that the torch itself is not modelled, as only the heat pool is necessary. As the influence of the two clamps on the final result is negligible, they were replaced by simply clamped boundary conditions.

Three-dimensional elements with eight Gauss points were chosen as shell elements do not allow to represent the effects on of the plate correctly. Eight gauss points were chosen as single Gauss point element induced hourglass modes.

One could also wonder why the simulation could not only be performed on a 2D plane perpendicular to the weld, thus neglecting longitudinal effects. This assumption was evaluated by Goldack [10], and he concluded that even if the longitudinal interactions are limited, their effect, most importantly on the residual stresses, can be significative. The 2D assumption was thus discarded.

The two interfaces whose contact have to be modelled here are the juxtaposed faces of the plates. As recommended in the LS-Dyna literature, a mortar type contact was used as the simulations were performed with an implicit solver [21].

At start time, five contacts are initiated at the location of the spotwelds, once the heat source passes over them, these contacts are overrun by a welding contact whose birth is whenever the temperature of the material goes beyond the 1300 Celsius degree threshold, which is the chosen melting temperature of the material.

4.3 Material model

The material model uses a multi-phase model, with a ponderation between the different phases of the material. In the present case, nine phases are defined: Austenite, Ferrite, Perlite, Bainite, Martensite, Base Material, Filler/Liquid, Tempered Martensite and Tempered Bainite. Each of these materials are defined steel phases, except for the base material one. This particular name is designed for the S355J2 steel, which is the only material modelled in Fabweld. As the reader may notice, the material used in the experiment is the S355MC. Unfortunately, the exact same material could not be found and performing a whole parameter identification process for the material used would have taken time that was not available. The base material will be used in this model as the initial material, and its parameters will be adjusted as much as possible to the actual material used.

Each of the phases has its own value of yield stress, heat expansion coefficient, heat capacity and heat conductivity that each evolve with temperature. The data comes from [1], which did experimented extensively on the S355J2 steel. All material properties will not be shown here, but they are all presented in the annex. The Young modulus, heat capacity and heat conduction coefficient are of interest however. Indeed, the Young modulus evolution, that can be seen Figure 4-e, is the same for all phases, except austenite and liquid material. All phases are assumed to be similar to ferrite for this particular variable. The liquid material Young modulus is obviously zero.

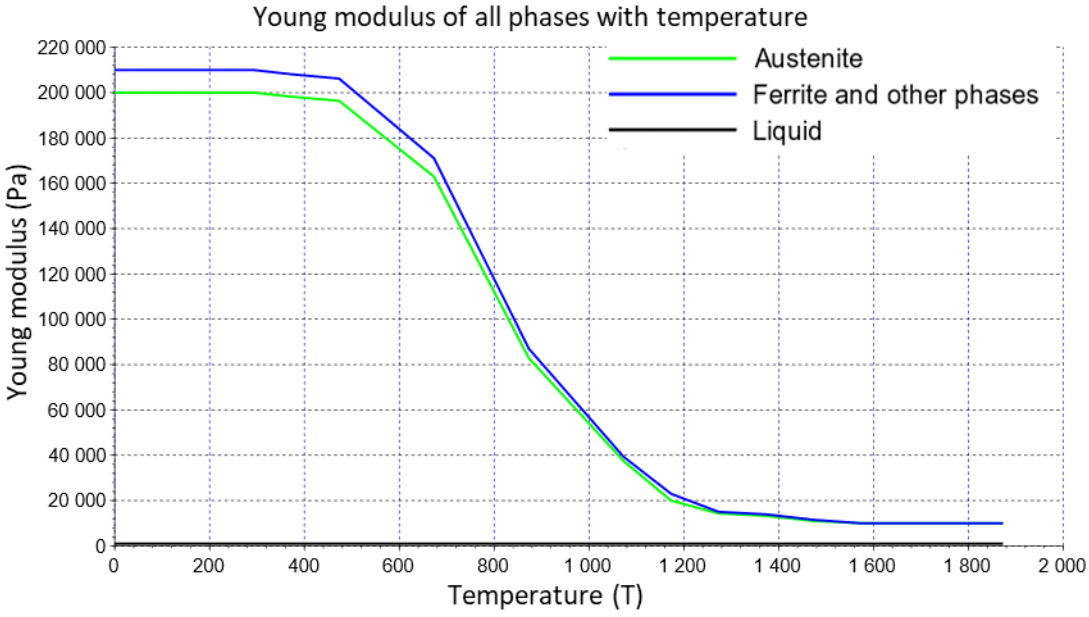

Figure 4-e: Young modulus of all steel phases present in the S355 of the model

The thermal properties of the material are, once again, based on past experimental data. It will be showed in the conclusion of this work that the thermal behavior of the modelled material is not exactly similar to the one used in the experiment, according to the simulation results.

4.3.1 Annealing model

A major feature of the model used in this paper is the annealing temperature, which is the temperature that, if reached, at which all plastic deformations and stresses will be reduced. This transition needs to be modelled, and needs a start temperature as well as an end one. A few models can be used to model the decrease in plastic strain, but the one used originally here is the simplest one : a linear decrease following Equation 1 where **n** refers to the phase that anneals, *a* to the *a*nnealing process, and ε_p to the plastic strain. In this particular model, a start

temperature of 1250 degrees and end temperature of 1300 Celsius degrees. This was chosen as is advised by Lindgren [4].

$$\varepsilon_p^n = \varepsilon_{p,start}^n \frac{T_a^{end} - T}{T_a^{end} - T_a^{start}}$$

Equation 1: Linear decrease in plastic strain for modeling the annealing process of the material

4.3.2 Phase transition model

Other than the annealing temperature, the phase transformation is a phenomenon that needs to be reproduced. In this manuscript, two main models are used : Koinstinen-Marburger (KM) and Johnson-Mehl-Avrami-Kolmogorov (JMAK). Both models are used primarily because of their time-saving features [22]. In further studies, with experimental phase measurement, the influence of such models is an interesting field to investigate. The reader should keep in mind that every decision made in the model are based on the FabWeld software. The decisions are justified in most cases, but the experimental data used for the transition model is not investigated.

Koinstinen-Marburger follows Equation 2, which is basically an exponential transition in between the phases. In this equation, x_a marks the concentration of the initial phase in the material and x_b denotes the concentration of the second one. T_{start} is a temperature, chosen to be the inception of the phase transition process. α_{KM} is a material parameter that is to be set by the user, and which is around 0.2 in this model. The exact value of the parameter can be found in the annex, as it may vary with the phases in question.

$$x_b = (x_a + x_b)\left(1 - e^{-\alpha_{KM}(T_{start} - T)}\right)$$

Equation 2 : Koistinen-Marburger (KM) model for steel phase transition in heating process

The KM model is mostly used for transitions that include a high cooling or heating rate, while Johnson-Mehl-Avrami-Kolmogorov is widely used for any other transformation, and can be seen on equation Equation 3.

The parameters $n(T)$ the exponent, $x_{eq}(T)$, the equilibrium concentration and $\tau(T)$, the relaxation time are curves defined by the data from [1]. As the model is the generalized JMAK approach, the temperature rate correction factors $f(\dot{T})$ and $f'(\dot{T})$, as well as the accelerator factor $\alpha(\varepsilon^p)$ are to be set by the user. $n(T)$ and $x_{eq}(T)$ in this manuscript, always have a value of one. $\tau(T)$ has a value in between 1e6 and 1. The $\alpha(\varepsilon^p)$ value has not been fixed

as it is a facultative parameter. Finally, $f^{(\dot{T})}$, $f'^{(\dot{T})}$ are mostly 1 except in the cooling situation, where they have an exponential-like growing value, as can be seen on Figure 4-f . Due to the parameters chosen here, the functions $f^{(\dot{T})}$ and $f'^{(\dot{T})}$ are the one regulating the phase change, following the experimental data [1]. Better modeling, following theoretical phase transformations laws, could be implemented [23]. Unfortunately, the metallography performed in this manuscript does not allow for phase disposition correlation. All parameter values that are not specified here can be found in the annex.

$$\frac{dx_b}{dt} = n(T)(k_{ab}x_a - k'_{ab}x_b)(ln\left(\frac{k_{ab}\,(x_a + x_b)}{k_{ab}x_a - k'_{ab}x_b}\right))^{\frac{n(T)-1}{n(T)}}$$

$$k_{ab} = \frac{x_{eq}(T)}{\tau(T)\alpha(\varepsilon^p)}\mathrm{f}(\dot{T})$$

$$k'_{ab} = \frac{1 - x_{eq}}{\tau(T)\alpha(\varepsilon^p)}f'(\dot{T})$$

Equation 3: JMAK model for steel phase transition in cooling process

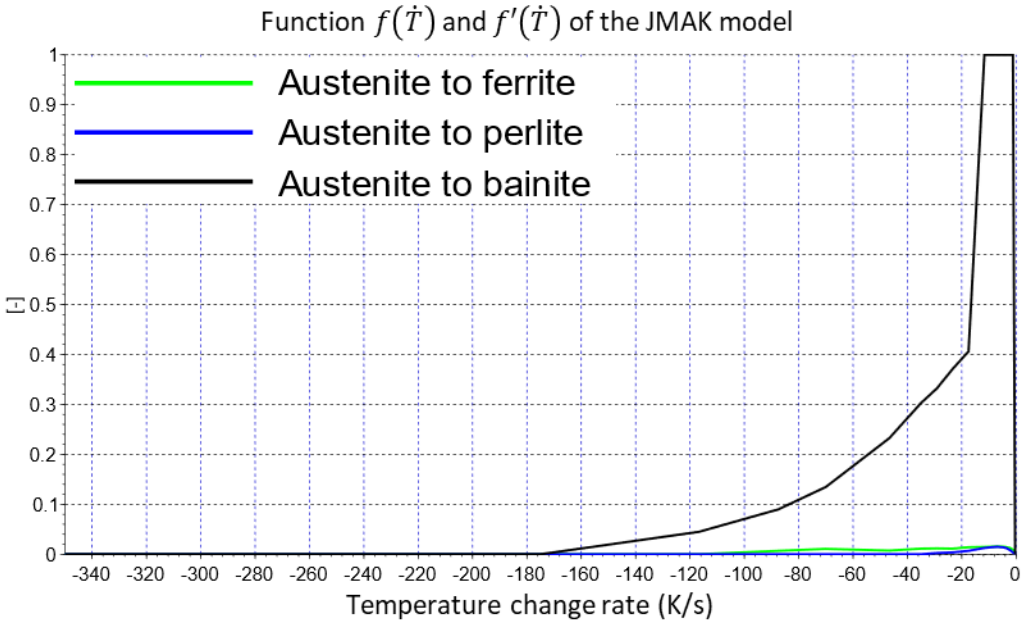

Figure 4-f: Function *f* regulating the JMAK model, *f'* has the exact same values

All the models used in between the phases can be seen in Table 2. The red color denotes the fact that the model is used during the heating process and the blue color for the cooling one. As the austenite is the phase that exists at higher temperatures, it is the only one for

which the cooling process is taken into account. JMAK is mostly used as it represents reality better, but MK is used in the case of the transformation from austenite to martensite.

FROM \ TO	**Austenite**	**Ferrite**	**Perlite**	**Bainite**	**Martensite**	**Tempered Martensite**	**Tempered Bainite**
Austenite		JMAK	JMAK	JMAK	MK		
Ferrite	JMAK						
Perlite	JMAK						
Bainite	JMAK						JMAK
Martensite	JMAK					JMAK	

Table 2: Phase transition models used in the material model, from the column phase to the line phase. Red text translates to the heating process and blue text to the cooling process.

4.3.3 Hardening flow curves

Another important parameter that happens during the phase transformation is the induced plastic strain, which is evaluated with the experimental data as well. Indeed, whenever a phase change occurs, the interaction within the material induces a certain level of plastic strain due to the difference in crystalline structure in between the phases. The form of the plastic strain induced by the phase modification can be seen in the annex as well.

Each of the phases has as well a hardening curve, which is, once again, coming from the same data [1]. For the base material, the flow curve can be seen on Figure 4-g . For the other phases, the flow curves can be seen in the annex as well.

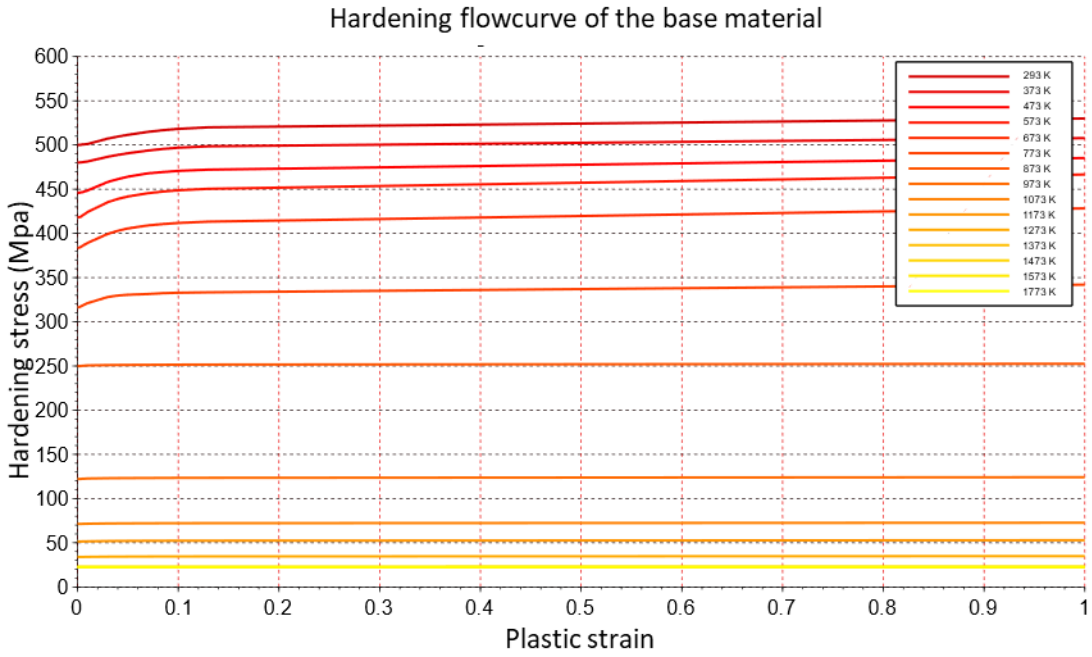

Figure 4-g: Hardening flow curves of the base material at different temperatures

4.4 Implicit solver

Both implicit solvers in this manuscript, the mechanical one and the thermal one, use for their equilibrium computation an automatically adjusted step size. Anytime the number of iterations exceeds the maximal number input by the user, the time step is reduced. On the other hand, if the number of iterations is lower than a standard value, it means that the timestep can be set to a higher value. Both the dynamic and the thermal solver are nonlinear, as a welding process includes a lot of nonlinearity.

The reader should keep in mind that the only solvers explored here are the ones present in the LS-Dyna software.

4.4.1 Thermal solver

The solver used for the non-linear solving of the thermal problem is the conjugate gradient method, with diagonal scaling used to scatter the work in between CPU's. The conjugate gradient method is a classical method used in equation solving [24]. This method

was chosen rather than Gauss's method to save computational time, and as no convergence issues were encountered.

The time integration is done using the classical implicit method (backwards Euler scheme) rather than the Cranck-Nichoslon scheme, due to the nonlinearity of the problem [21]. However, both schemes were tested and no significative change in temperature or CPU time was visible.

4.4.2 Mechanical solver

The dynamic solver used for the space discretization is named "nonlinear with BFGS updates" in the LS-Dyna literature, it is a complex solver using different line search methods. If the reader is seeking further information, he/she is advised to explore LS-Dyna's keyword manual [21].

Due to the nature of the problem, oscillatory motions and inertial forces are not present. To reduce the computational time, a static analysis was chosen. Thus, at each time increment computed by the thermal solver, the mechanical solver will try and reach the static equilibrium of the model.

4.4.3 Coupling of the solvers

The default thermo-mechanical approach of LS-Dyna is the 2-way coupling approach, also called staggered weak approach. This means that the thermal and mechanic solver work in parallel while exchanging information. This accounts for every coupling that occurs between the two domains. A diagram of the process can be seen on Figure 4-h. As can be seen on the figure, the mechanical timestep should be smaller than the thermal one, as if it is not the case the mechanical solver could be blinded to the information that a thermal step was providing.

The information transmitted by the mechanical solver to the thermal one could be mostly neglected, as the heat input by the torch is far greater than the one due to mechanical mechanisms. In this case, the model is called 1-way coupling. In the present model, a 2-way coupling will be kept as an important information has to be transmitted by the mechanical solver: the geometry of the problem. Indeed, the nodes on which the heat is applied will move due to the thermal expansion of the material. These nodes still are subject to the heat input, this creates thus a coupling : the thermal expansion moves the location of the welding boundary condition.

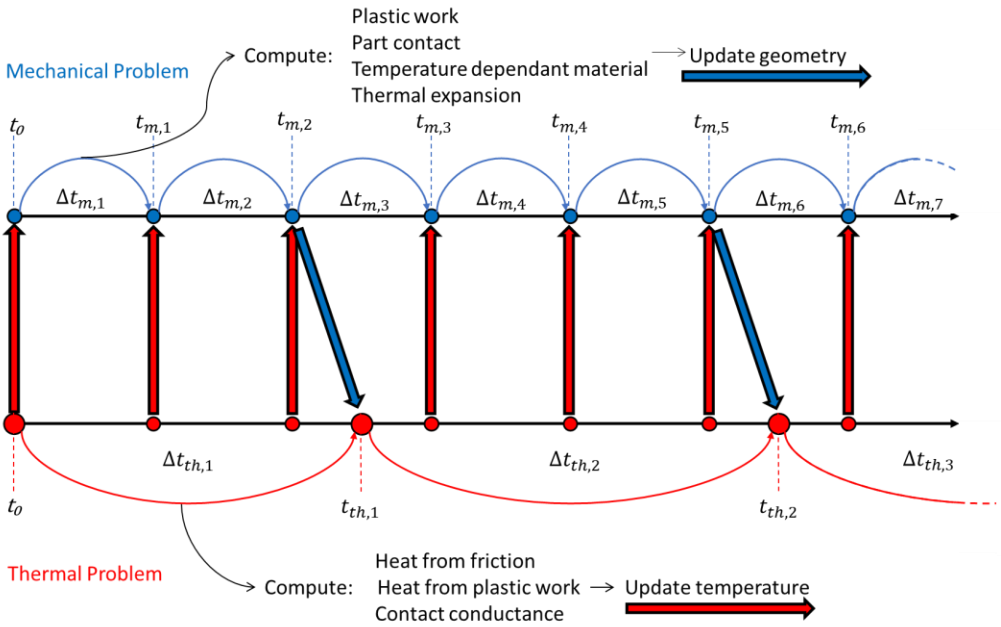

Figure 4-h: diagram of the thermo-dynamic coupling between the solvers

4.5 Boundary conditions

4.5.1 Radiation and convection

The radiation coefficient can be computed as the product between the Stefan-Boltzmann constant σ and the emissivity ε. As seen on equation , the emissivity value of steel is taken as 0.35 [25], the resulting radiative coefficient is

$$h_{rad} = \varepsilon\,\sigma = 0.35\ 5.67\text{e}-8 = \ 1.9845\text{e}-8\,\frac{W}{K\ m^2}.$$

Equation 4: Radiation heat coefficient definition

Equation 5 is depicting the formula used to compute the free convection of an horizontal plate. The parameters *g*, β, α, ν are the gravitational acceleration, and characteristics of the air: its thermal expansion coefficient, thermal diffusivity and kinematic viscosity. Their value can be seen in Table 3 . L is the characteristic length of the hot surface, which is not easy to determine as the plate is not heated homogeneously over the whole surface. For the same reason T_s, the surface temperature, cannot be defined easily. T_∞, the air temperature, is fixed to the temperature measured during the experiment.

$$a_L = \frac{g\,\beta}{\alpha\nu}(T_s - T_\infty)L^3$$

$$\overline{Nu} = 0.54Ra_L^{0.25}$$

$$\overline{Nu_L} = \frac{\bar{h}L}{k}$$

Equation 5: Free convection over a hot horizontal plate heating coefficient [26]

Parameter	Unit	Value
g	$\frac{m}{s^2}$	9.81
β	$\frac{1}{K}$	0.00369
α	$\frac{m^2}{s}$	0.00002141
ν	$\frac{m^2}{s}$	0.00001349

Table 3: Physical properties of air at 25°C

As a unique convection coefficient has to be defined over the whole plate, rather than using a predefined value, it will be modified to stick with the experimental values. If the whole plate is heated at 1300 degrees, which is the maximal value at the weld, the thermal coefficient is 11.6$\frac{W}{m^2K}$,. If it is heated at 50 °C, such as at the end of the experiment, the coefficient is 6$\frac{W}{m^2K}$,. The first guess coefficient is thus chosen coefficient is 7 $\frac{W}{m^2K}$, as the plate is most likely overall closer to 50°C homogeneously.

Alternatively, a convection coefficient computed adaptively all along the modeling is a better model, which was not implement here, it is however expected to result in more similarity between the model and the experiment [27].

4.5.2 Embedded Boundary conditions

As stated before, the clamps of the experiment are not reproduced in the model, due to the almost non-existing influence it has on the final results. However, the rigid body modes of the plates have to be removed, this is why the location where the clamps should have been are simply constrained in all directions and all rotations.

4.5.3 Heat input boundary condition

As the heat input is considered to be a boundary condition, it will be addressed here. As stated previously, a double-ellipsoid shape with a constant distribution over the front part and another constant distribution on the rear part will be used. The dimensional parameters were chosen to stick with what has been observed in the experiment, they thus will be addressed in the correlation section.

The intensity of the heat input to the model is a variable that has to be calibrated when corroborating the model to the experiment. The first guess should be the theoretical input of the TIG welding process, given by Equation 6. Where Q is the heat input (W), U is the tension (V), I is the current (A) and η is the TIG efficiency, which is around 70%.

$$Q = \eta\, U\, I$$

Equation 6: theoretical heat input of the TIG process [7]

Using this equation, one can define the theoretical value of the heat input for both experiments. As a recall: both experiments have the same efficiency, weld speed and voltage of respectively 0.7, 3.33 mm/s and 15 V. The only difference is in the amperage: 120 A for the first experiment and 110 A for the second one. This develops into a heat input of 1260W for the first experiment and 1155 W for the second one.

4.6 Element size and disposition

The major restrictive factor in the meshing of the components is the thickness of the plates. At least three elements were necessary to fully represent the heat effects of the welding process, and upwards number of elements on the thickness should be investigated. As the priority of this manuscript was to reach surface thermal similarity, the mesh independence study was first performed on the length and width of the plate.

The number of elements on the two other dimensions: could thus be modified to perform a mesh independence study. The same size of element is imposed on the width and length of the plates. The particularity of the model is that a finer mesh near the heat input, a bias was thus imposed on the length of the plates, it can be seen in Figure 4-k.

Figure 4-i shows the evolution of the plate extremity displacement with a finer mesh, and the CPU computation time to reach the same process. Past 100 elements on the width (and 100 elements per 200 milimeters for the length), the solution does not evolve in a manner that

would justify using that much more time. This mesh dimensions were thus chosen , and the final result can be seen on Figure 4-j.

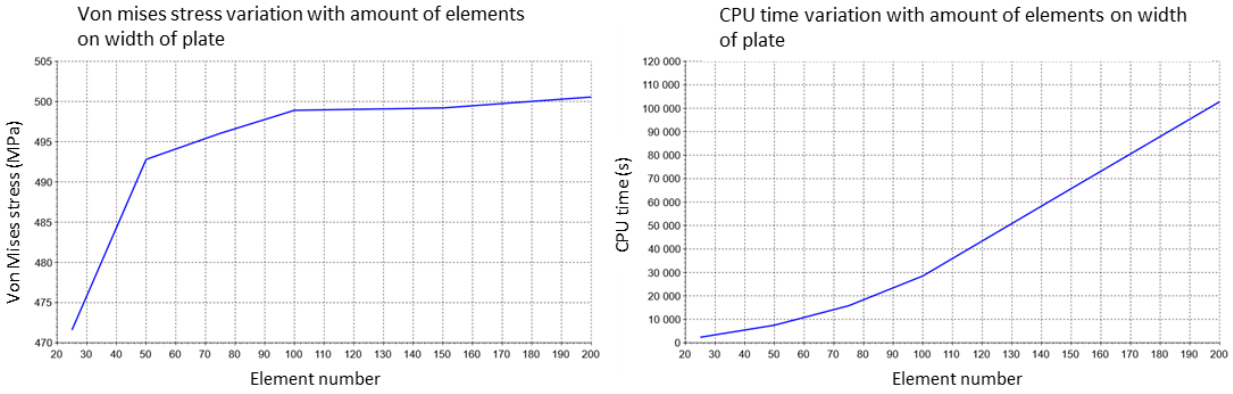

Figure 4-i: Mesh independence study of the model, taking into account the CPU time needed to compute Von Mises stress

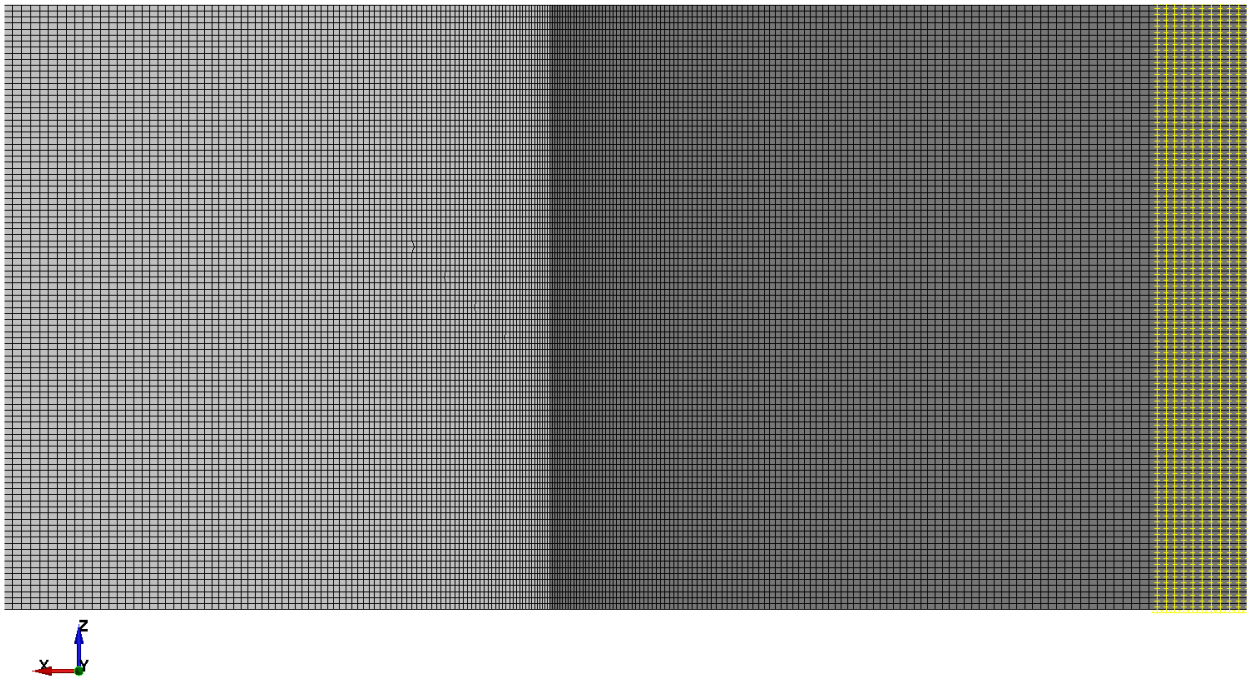

Figure 4-j: Final model disposition, with nodes constrained in their six DOF's highlighted in yellow

Figure 4-k: Element distribution through the thickness of the small plate

5 Tool development

5.1 Heat pool measurement

The two major measurements that characterize the heat pool are the width and the deepness(also called penetration). Once they are found, the weld pool shape is defined, but the heat distribution is still to be determined. Figure 5-a is a metallography of the singular plate of the second experiment. And will allow to compare the HAZ of both the model and the experiment to determine the heat distribution model.

The reader remembers the double ellipsoidal shape that is used to input heat in the model, the measurements of said shape are based on the present metallography. Thus, a width of 2.30 millimetres on each side is set, and according to [13], convention states that the semi-axis in front of the ellipse should be equal to the width and the semi-axis at the back should be two times as large. This basically means that the front part of the ellipse is 2.3 millimeters long and that the rear part is 4.6 millimeters long. Finally, as a deepness of 1.54 millimetres was reached, as can be seen on the metallography. These parameters are taken for the two models, the one representing the first experiment as well as the one representing the second. To improve the model of the first experiment, an independent metallography can be done.

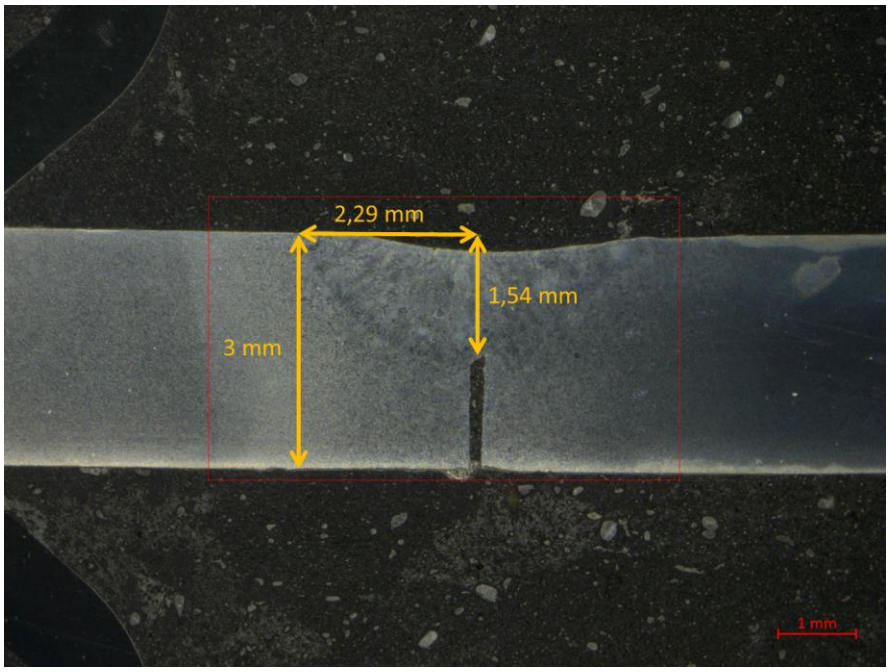

Figure 5-a: Metallography of the cross section of the second experiment, with the heat pool dimensions highlighted in yellow

As the reader may notice, the weld pool is not exactly symmetrical from the point of view of the plate interface. Indeed, there is a slight leftwards offset. This should be kept in mind as it could induce errors between the model and the experiment.

5.2 Thermal history analysis

The heat history found by the first experiment is unfortunately the sole measure that can be correlated, due to the unreliability of the displacement results. The mean thermal output can be seen on Figure 5-b, with the standard deviation depicted with the black dashed lines. The thermal output of the first experiment will be correlated to the model rather than the second experiment due to the higher number of tests done, which improves the reliability of the data.

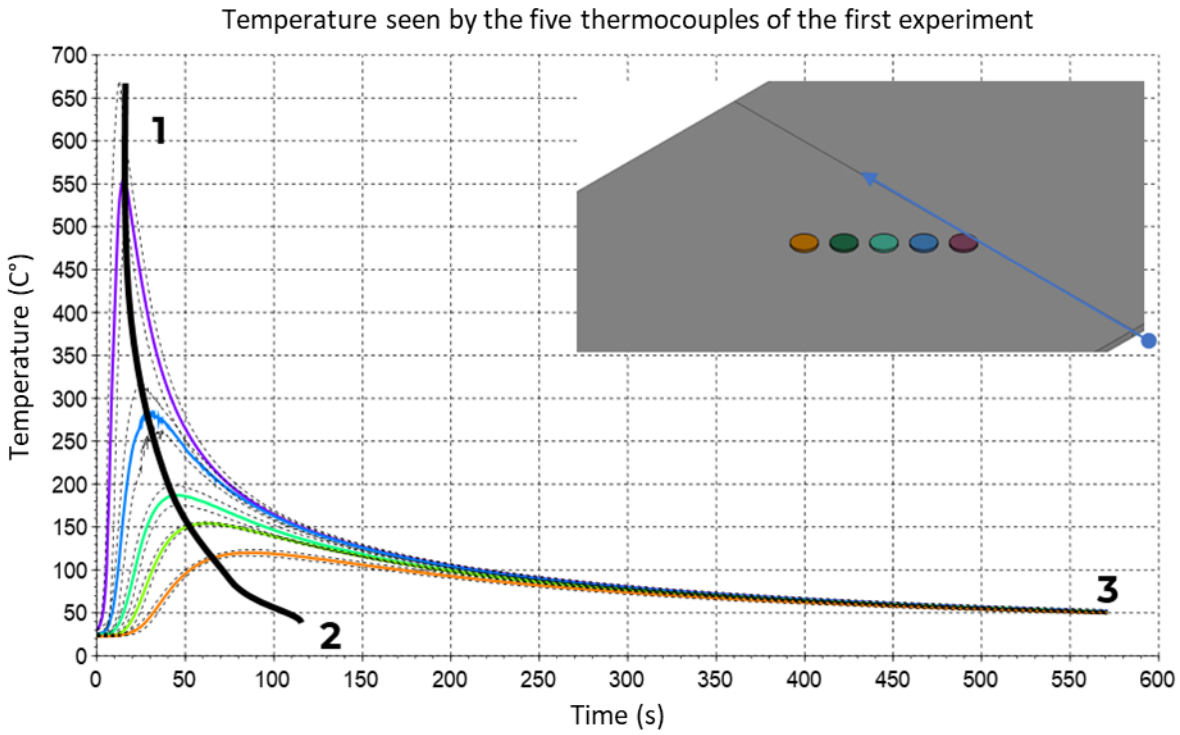

Figure 5-b: Mean thermal output of the five thermocouples of the first experiment, with standard deviation in blacked dashed lines

The three main features that the temperature history of the first plate describe are marked on Figure 5-b. The first notable value is the maximal temperature perceived by the first thermocouple, at 5 mm from the weld. Its value is 551°C, far from the 1300 degrees required

for the steel to melt. This value, with the fact that the weld pool is 2,5 centimeter wide, shows how steep the temperature gradient is close to the weld line.

The second feature of this thermal data is the fact that the peak perceived by the thermocouples seems to be offset in time as we measure further from the weld. This is explained by two phenomenon: the time offset is an addition of the time required by the torch to reach the next thermocouple coordinate and of the time required for the heat to travel through the material from conduction.

Finally, one of the most notable features is that the final perceived temperature is the same, 50°C, at all thermocouples after ten minutes of processing. The plate temperature can thus be assumed homogeneous. This is mainly due to compensation: the higher the temperature is, the higher the radiation and convection coefficient grows, and the higher is the amount of heat lost to air.

To assert the relevance of the data generated during the first experiment, an analysis on the standard deviation is to be done. For this purpose, the data retrieved by the first and last thermocouples can be seen on Figure 5-c and the standard deviation data for all thermocouples is visible on Table 4. It is important to note that the standard deviation during the cooling phase is always smaller than the one of the peak temperature of the corresponding thermocouple.

What can be taken from this data is that, due the heavy temperature change, high standard deviation can be seen during the heating phase, and even more so for the first thermocouple, who is subject to higher temperature change. In opposition, the cooling phase and peak temperature of all thermocouples have reliable value as the standard deviation is no higher than 11% in the worst case. The conclusion is thus that this data set is quite reliable, but the heating phase needs to be evaluated with a critical mind.

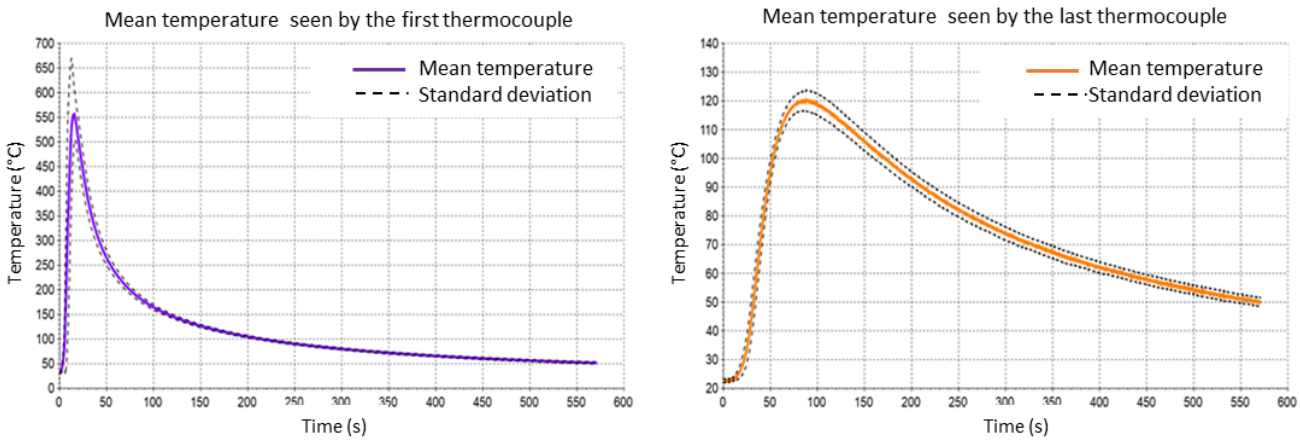

Figure 5-c: Temperature seen by the first and last thermocouple during the first experiment

Standard deviation	**5mm**	**15mm**	**25mm**	**35mm**	**45mm**	
Heating phase	81%	48%	26%	21%	16%	
Peak temperature	11%	6%	6%	1%	3%	

Table 4: Standard deviation value along the different thermocouples during the heating phase and at peak temperature

5.2.1 Correlation

The first best guess at a modeling of this experiment is done using all theoretical and experimental values defined earlier in the manuscript. The only real unknown is the convection coefficient, with was set to seven, as stated before. The resulting correlation can be seen on Figure 5-d.

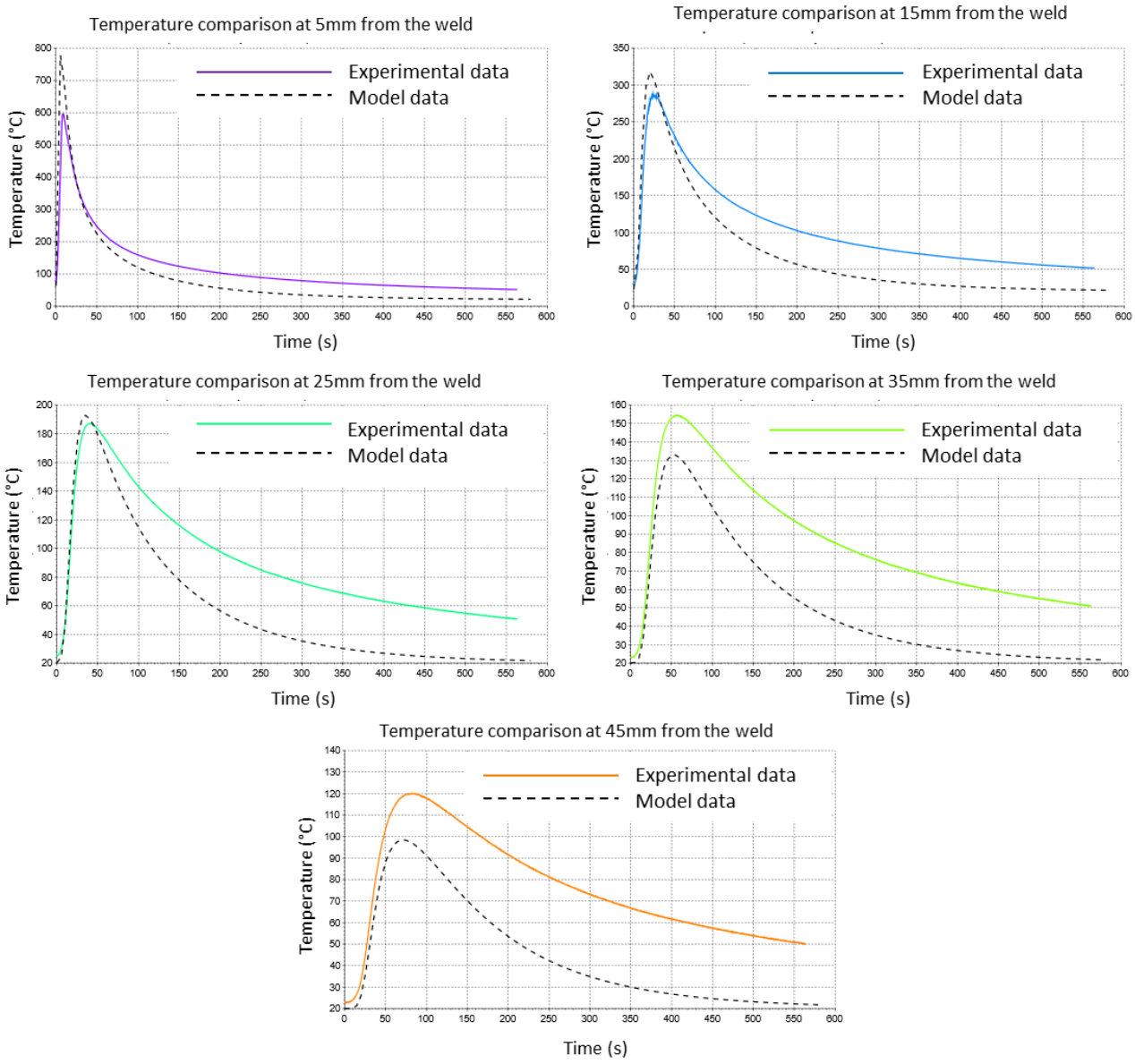

Figure 5-d Temperature correlation of the first experiment and the model with all parameter set to the theoretical first guesses

The main problem the model seems to present is an overshoot in the heat dissipation to air. Indeed, even if the peak temperature seen by the first thermocouple is overshot by almost 30% of the experimental data, the temperature peak of the last thermocouple is underestimated by 20%. This is a clear indication that too much heat is given to the environment of the plates. Another factor that supports that idea is the fact that the temperature difference between the final temperature of the model and the one of the

experiment is staggering: almost a 30°C leap. A lower convection coefficient should be able to perform the change in heat dissipation wanted, and lowering the heat input should allow us to reduce the peak temperature of the first thermocouple to the right value.

5.2.2 adjustment

These two parameters were thus modified according to Table 5. As the reader can notice, the convection had to be overall neglected for the thermal history of the material to be reproduced. This assumption is clearly not physical, and even if the present set of parameters give satisfyingly similar results to the experiment, a critical mind should be kept.

Parameter	Heat input (W)	Convection coefficient
Theoretical value	1260	7
Final value	1000	0

Table 5: Adjustment of the parameters for better similarity of the temperature history

The similarity between the temperature history of the piece can thus be seen on Figure 5-e. the magnitude of the temperature is consistent with the magnitude perceived in the experimental tests. The overall cooling process of both model and experiment are close as well, with a slightly colder plate for the model. This could be fixed by reducing the dissipated heat slightly, which could be performed with the radiation coefficient.

This good correlation between the model and the first experiment confirms that the TIG welding process, with the specific parameters and disposition used in this manuscript, can be thermally reproduced, but with some reserve. Indeed, two parameters have been modified out of their theoretical values. The convection phenomenon had to be completely ignored, which is not physical. The most likely cause of this effect is that the heat conductivity and capacity of the model are not at the exact value of the experimental material. Modifying these two parameter would most certainly show that the convection is not to be ignored.

Now that it is stated that the temperature history of a welding process can be reproduced, this model can be applied on the second experiment.

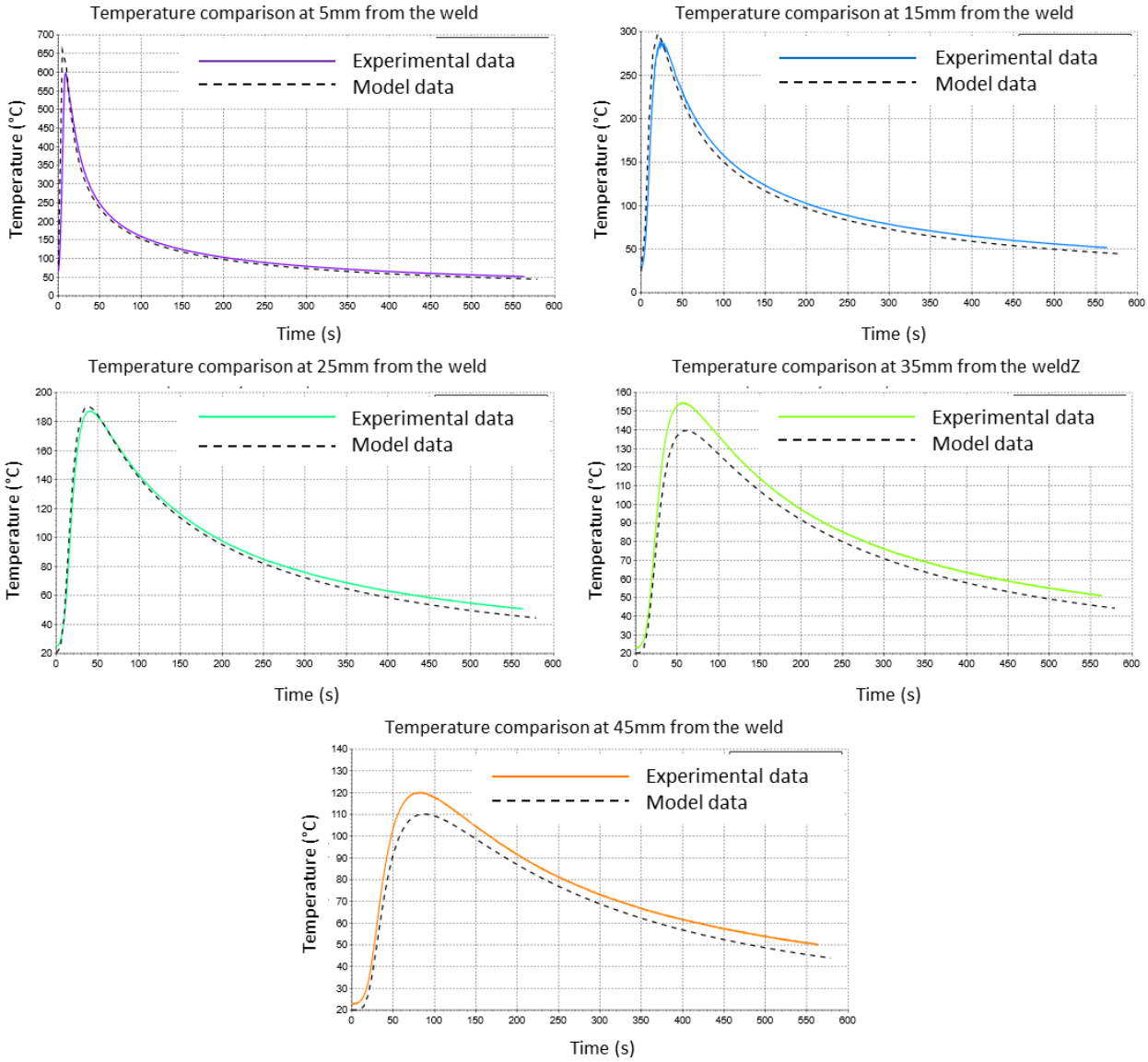

Figure 5-e: Temperature history comparison in between the adjusted model model and the first experiment

5.3 Displacement analysis (Second experiment)

5.3.1 Data identification and comparison

As stated previously, the second row of experiments had as output only one singular plate with a one-shot weld. The other plates had to be re-passed to be welded on the whole length. The rest of the experimental process was the same.

Figure 5-e shows the difference in temperature history of the first and second experiments. As a reminder, the only parameter that has been changed is the amperage, that has a value of 120 A at first, and then 110 for the second experiment. This slight change in input heat obviously an influence on the peak temperature perceived by the thermocouples.

However, as can be identified on the graphs, the second experiment peak temperature for the first thermocouple is almost 62% of the value of the first experiment, whereas it increases to 90% of the value for the furthest thermocouple. This is due to a phenomenon already addressed earlier : the higher the temperature, the higher the heat coefficient, the most is the heat passed through air.

The reader should note as well that the final temperature of both experiments at all thermocouples is 50°C. Which is once again due to heat dissipation.

The main conclusion that can be withdrawn from this comparison is that the amount of heat given to the material has a major impact on the temperature close to the weld, but the behavior further from the weld line is very similar in amplitude.

Such a conclusion should give us as indication that a similar adjustment would be needed in the case of the second experiment than in the first one. This will prove to be incorrect further in the development of this manuscript.

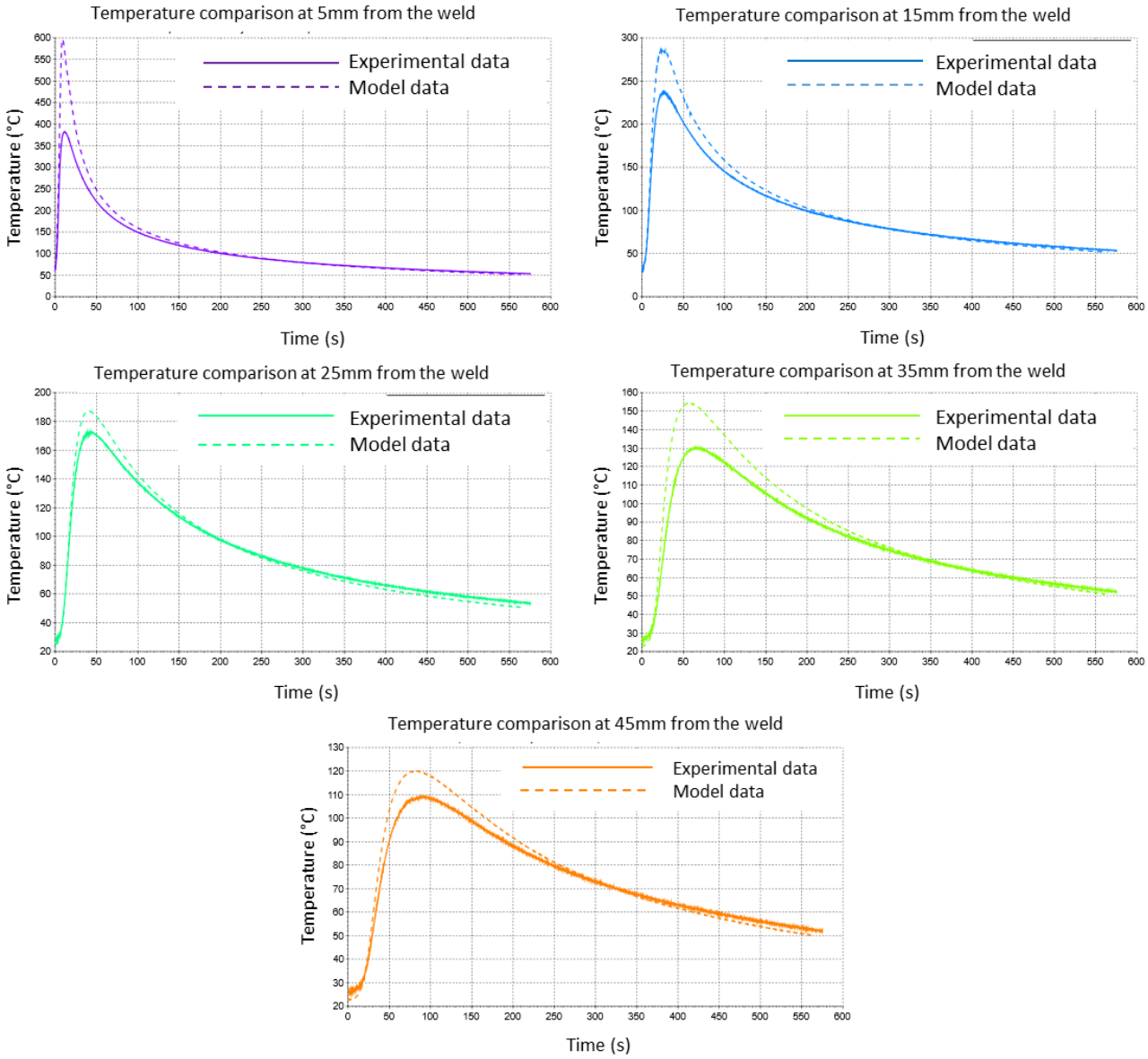

Figure 5-f: Thermal history comparison between the five thermocouples of the first and second experiment

On an other hand, the displacement retrieved by the second experiment can be seen on Figure 5-g.

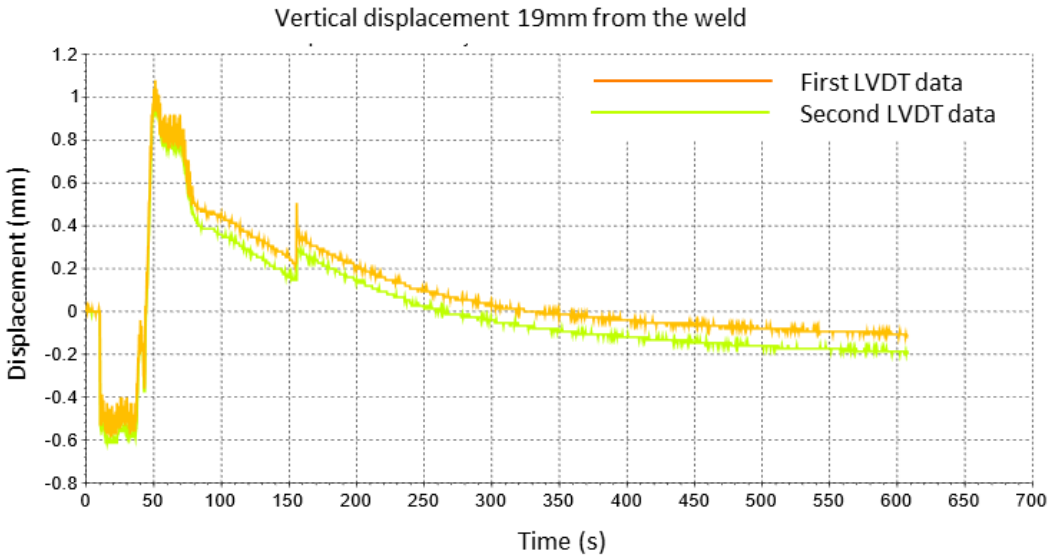

Figure 5-g: Displacement data seen by the LVDT's in the second experiment

As explained previously, displacement in a weld is due to the thermal expansion of the material to be welded. In the present case, the first downwards displacement is due to the expansion of the molten steel, as well as the gravity's force, as depicted on Figure 5-h. The orange half-circle represents the weld pool and the gray rectangles represent the plates.

Figure 5-h: Beginning of process negative displacement of the plates depiction

The second, upward displacement is present because of the thermal shrinkage of the material, which induces stresses and strains notably due to phase modification. This phenomenon is depicted on figure Figure 5-i.

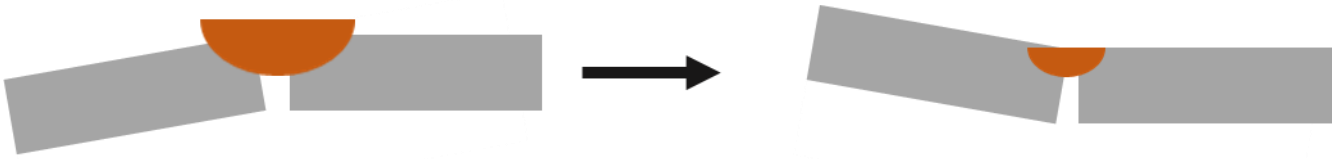

Figure 5-i: second (positive) displacement of the plates, a depiction

Finally the processing negative displacement happening after the end of the welding process has no physical explanation as of now in recent publications. A rational hypothesis would be the reduced bending resistance of the plate due to heat, as the more the plate cools down, the smaller the displacement is.

5.3.2 Correlation

Once again, a first guess of the model was performed with all theoretical parameters. The resulting temperature correlation can be seen on Figure 5-j.

Overall, the issues found in the model are with no surprise comparable to the ones of the first experiment: the first temperature peak is too high, the last one too low, and the final temperature is underestimated by the model.

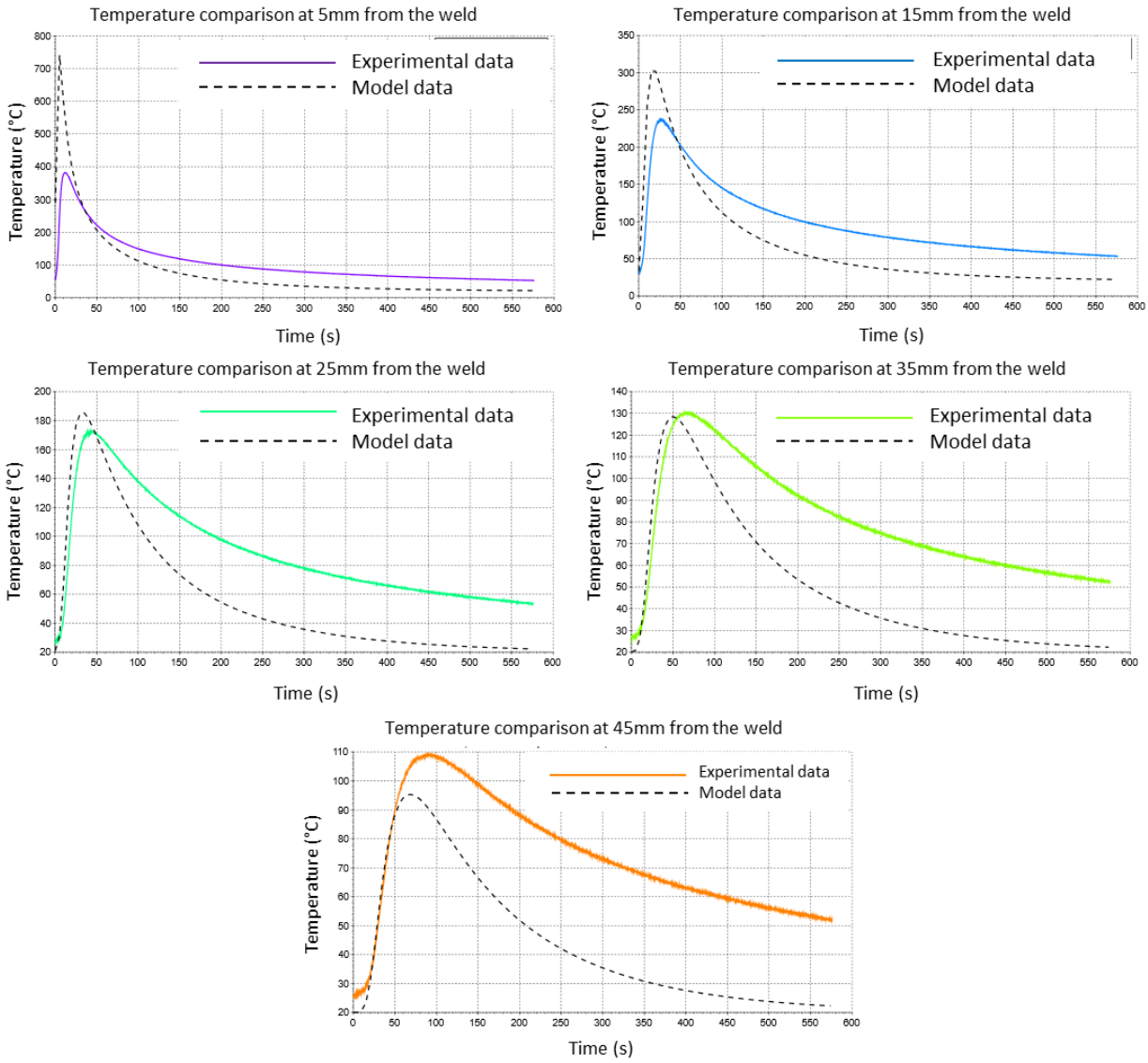

Figure 5-j: Temperature correlation of the second experiment and the model with all theoretical first guess parameters

The displacement correlation can be seen on figure Figure 5-k. The model shows the same tendencies in displacement: an initial downwards displacement followed by an sudden upwards one, ending with a slow negative displacement once again. This can lead to the conclusion that physically, the experimental displacement could be represented. However, a major issue shows here, the negative displacement on either the first or third phase on the

graph has a magnitude multiple times what was found in the experiment. Adjusting is thus necessary.

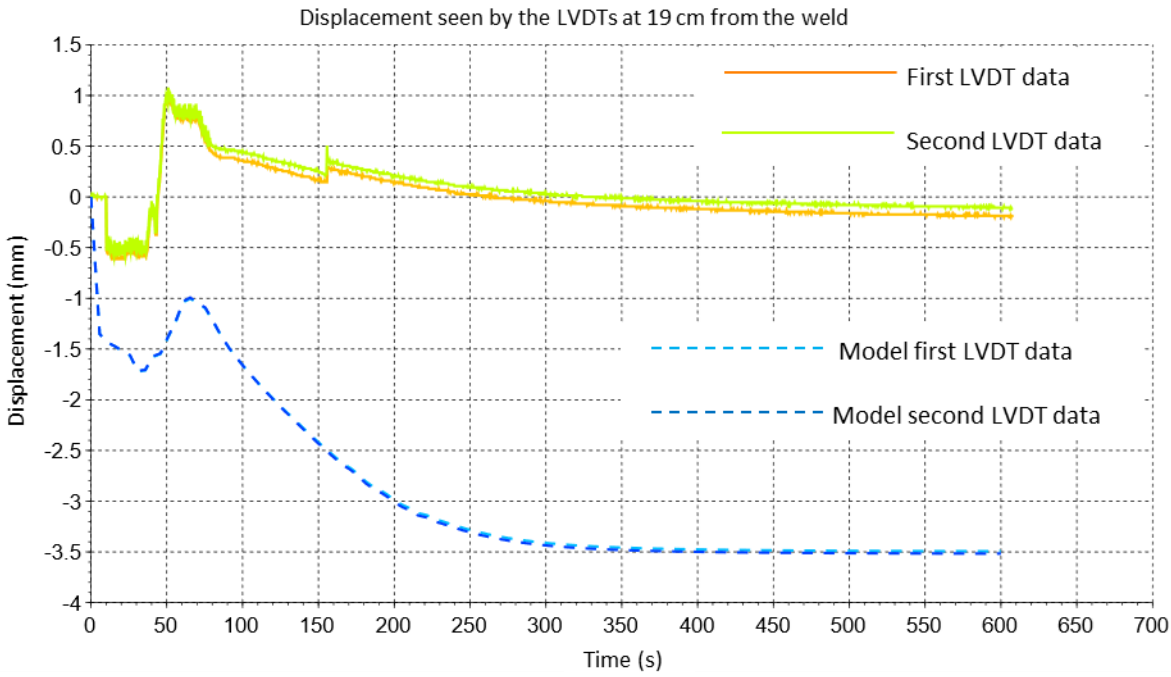

Figure 5-k: Displacement correlation of the second experiment and the model with all theoretical parameters

5.3.3 Adjusting

The first logical step here, to adjust the temperature profile, would be to neglect the convection coefficient, as was done for the model of the first experiment. Unfortunately, this modification gave insufficient adjustment of the results: too much heat was still getting through to air, as can be seen Figure 5-l.

As this hypothesis of the neglection of the convection coefficient was not confirmed for the second experiment, it should be set aside for the model overall, and a modification of the heat capacity and heat conduction in the material should allow for a non-zero constant convection coefficient. Another lead that can be pursued is the one of the variable heat coefficient, as here a single value is defined on the whole plate, which is not extremely precise.

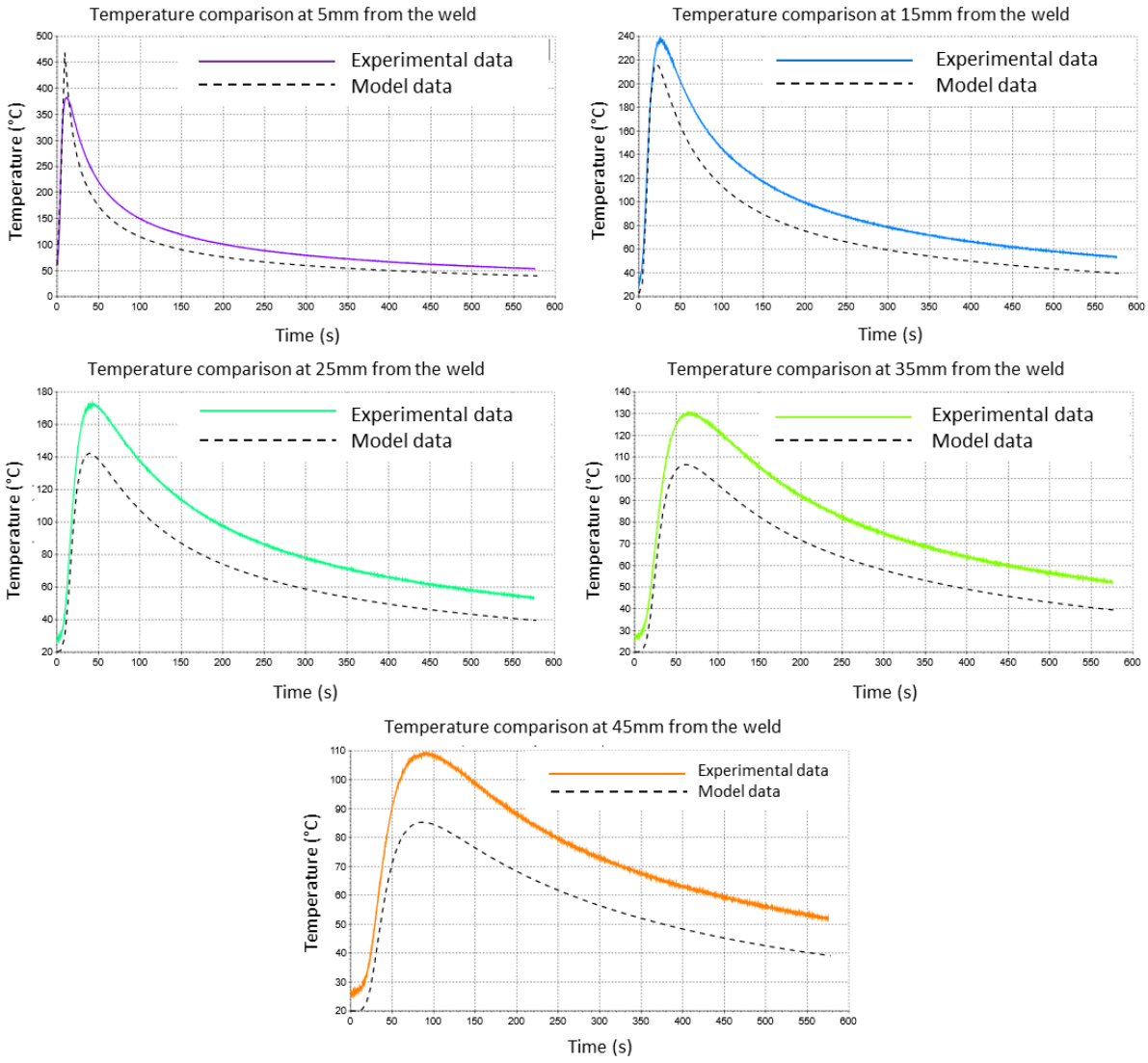

Figure 5-l: Comparison of the second experimental thermal history results and the first adjustment of the second experiment model

To further the adjustment, the influence of a few parameters, that have been presented earlier, have been analyzed. The resulting influence matrix can be seen on Table 6. To reach a good similarity between the experiment and the model, the thermal behavior of the material should thus be under investigation. This might not come as a surprise, as the experimental data used in the model does not come from the exact plates that were used for the experiment.

The matrix of influence has been developed through verification of the parameters in the model, but they could be obviously justified physically.

A heat input increase has the same effect as the change in amperage had between the experiments. As more heat comes into the material, the temperature increases. As the convection and radiation coefficient grows with temperature as well, the influence further down the transverse direction is lower, the last thermocouple thus sees a lower increase in temperature. This adaptation of the convection and radiation has as effect as well that the final temperature of the plate is still 50°C.

The increase in convection & radiation coefficient has no effect on the peak temperature of the closer thermocouple, as convection has a short amount of time to take place. But as the time and distance grows, their influence does as well. The increase in the coefficients translates to a greater amount of heat given to air, which thus reduces the temperature of the plate.

As the heat capacity of the material grows, the amount of heat necessary to raise the temperature of said material is more important. That is why the overall temperature seen by the fist thermocouple is diminished. As this happens, the influence of temperature on the convection coefficient takes places and less heat is given to air. The conduction in the material thus takes place and the peak temperature of the last thermocouple increases.

Finally, the increase in heat conduction will have as effect that the overall temperature will be better scattered in the plate, thus a reduction in the first peak and a increase at the last one.

Parameter to increase	**First thermocouple**		**Last thermocouple**	
	Peak temperature	Final temperature	Peak temperature	Final temperature
Heat input	+	=	+	=
Convection & radiation coeff.	=	-	-	-
Heat capacity	-	=	+	=
Heat conduction	-	=	+	=

Table 6: Influence matrix of the different thermal parameters included in the model, that can be adjusted to reach similarity between the model and experiment

Once the thermal history is reproduced sufficiently well, the adjustment of the displacement can be performed. The main parameter that could influence on this displacement is obviously the thermal expansion of the material.

6 Conclusion

The main goal of this manuscript is do define a methodology allowing to use FEM simulated welds, or at least their outputs, in greater-scale models, where the actual welds are not the phenomenon of interest but could have an influence. Indeed, the thermo-mechanic nature of the welding process induces residual stresses that could affect the overall resistance of a structure for instance.

The methodology that has begun to be developed here is detailed hereafter:

1. State of the art
2. Tool definition
3. Tool development
4. Influence of tool parameter modification
5. Tendency reproducibility in experimental setup
6. Implementation of the tool in another model and behaviour analysis

As stated in the introduction, the objective of this paper was to develop the numerical tool to allow further testing . This was set into motion here by comparing an finite element model output to two separate experiments.

The first experiment allowed to stated that the temperature of the plate is reproductible. To reach this temperature similarity, the heat input had to be tuned, which was expected. However, the free convection over the plate had to be ignored, which was not expected and has no physical justification.

The second experiment, with a different heat input, allowed to determine that the adjustments found on the first model could not allow to reach a good temperature history similarity for all cases. The model thus requires further adjustment, with a lead being found through the thermal parameters of the material and the convection and radiation coefficient value.

7 Future work

As the work done in this manuscript is designed a springboard towards future work, further analysis and tests that could be done are numerous. This section will be divided in two parts: one where the work done would have as objective to refine what has already been done in the methodology, and one where the research would use the work of this manuscript to move along in the methodology.

7.1 Refining the present work

To increase the reliability of the model presented in this paper,

- A thickness-wise element study can be performed
- Further adjustment can be performed to reach deformation similarity
- Implementation of a temperature-variating convection and radiation coefficient could change the adjustment necessary.
- Further metallography, with a finer polish and a more sophisticated microscope, could allow to seen phases in the weld. This would allow to determine if the phase transition model is reliable.
- Material testing could be done on the exact samples used in the experiment

7.2 Further down the methodology

The next step is to set the boundaries for the model used here. Almost every parameter that the TIG welding offers should be investigated: weld speed, voltage, amperage, torch direction and more. Every parameter that the plates offer is a subject to be concerned with as well: plate thickness, material, preparation of the plate, etc. Finally, the process itself can be changed. From TIG to electron beam welding, or stir welding, and more.

Mostly, the scope in which the model is convenient is for now very narrow, as only one set experimental parameters has been investigated. It should be enlarged for the model to be relevant in the industrial practice.

8 Acknowledgements

To Mr. Senart, my thesis supervisor, for his continuous help and availability and his many practical answers to my many questions.

To Mr. Peters, Mr. Goldoni and most especially Mr. Bruno, who helped me with their knowledge in the workshop, and allowed me to perform the experiments needed for my thesis.

To Mr. Sanchez-Garcia, who took time of his schedule to answer my questions and perform the metallography.

To Mrs. Cofano, Mrs. Svarova, Mr. Renard, and the whole IDEAS branch of CRMGroup, who cleared many of the interrogations I had and provided an ideal work environment.

To Professor Ponthot, of the university of Liège, for his insights and expertise on the finite element method

9 Bibliography

[1] M. Wichers, "Schweißen unter einachsiger, zyklischer Beanspruchung Experimentelle und numerische Untersuchungen," 2006.

[2] K.Masubuchi, Analysis of welded structures, Elsevier, 1980.

[3] M. Ninshu and D. Deng, "Welding mechanics analysis of countermeasures for product performance problems," in *Welding deformation and residual stress Prevention* , 2022, pp. 309-356.

[4] L.-E. Lindgren, "Finite element modeling and simulation of welding," *Journal of Thermal Stresses,* vol. 24, pp. 141-192, 2001.

[5] S. Liu, A. Kouadri-Henni and A. Gavrus, "DP600 Dual Phase Steel Shermo-elasto-plastic Constitutive Model Considering Strain Rate And Temperature Influence On FEM Residual Stress Analysis Of Laser Welding," *Journal of Manufacturing Process,* vol. 35, pp. 407-419, 2018.

[6] B. Ali, M.-Z. Marjan, C. Ahmad and J. Mohammad, "Finite element modeling of the electron beam welding of Inconel-713LC gas turbine blades," *Journal of Manufacturing Processes,* vol. 26, pp. 339-354, 2017.

[7] P. Svarova, *Soudage TIG,* vol. Internal report, CRMgroup, 2021.

[8] R. Rishi, N. Ramesh, R. Santosh, A. Nitin, R. Vinod and S. Ajaypal, "Experimental Investigation and Optimization of TIG Welding Parameters on Aluminium 6061 Alloy Using Firefly Algorithm," in *Material Science And Engineering*, 2017.

[9] T. Klöppel, "Simulating Thermal-Mechanical processes with LS-Dyna," in *DYNAmore express Webinar Series*, Stuggart,Germany, 2020.

[10] J. Goldak, B. Patel, M. Bibby and J. Moore, "Computational weld mechanics," in *AGARD Workshop Structures and Materials 61st Panel meeting,*, 1985.

[11] G. Rubio, D. Giarollo, J. Mazzaferro and C. Mazzaferro, "Prediction of angular distortion due GMAW process of thin-sheets Hardox 450® steel by numerical model and artificial neural network," *Journal of Manufacturing Processes,* pp. 1202-1213, 2021.

[12] T. Loose and J. Rohbrecht, "Equivalent energy method for welding structure analysis," in *11th European LS-DYNA Conference* , Salzburg, Austria, 2017.

[13] M. Rikken, G. Montalbini, B. Frydman and D. Gration, "Demontrating LS-Dyna's Capabilities in Welding Simulations by experiments," in *16th International LS-Dyna Users Conference*, 2020.

[14] S. Thompson and G. Krauss, in *31st Mechanical Working and Sreel Processing Proceedings*, Warrendale,PA, 1990.

[15] J. Ping, W. Chaochao, Z. Qi, S. Xinyu, S. Leshi and L. Xiongbin, "Optimization of laser welding process parameters of stainless steel 316L using FEM, Kriging and NSGA-II," vol. 99, no. 147-160, 2016.

[16] M. Islam, A. Buijk, M. Rais-Rohani and K. Motoyama, "Process parameter optimization of lap joint fillet weld based on FEM–RSM–GA integration technique," *Advances in Engineering Software,* vol. 79, 2015.

[17] H. S. Mohammad, A. Mostafa and A. Parviz, "Multi Objective Optimization of Friction Stir Welding Parameters Using FEM and Neural Network," *International Journal of Precision Engeneering And Manufacturing,* vol. 15, no. 11, pp. 2351-2356, 2014.

[18] D. Deng and H. Murakawa, "FEM prediction of buckling distortion induced by welding in thin plate panel structures," *Computational Materials Science,* vol. 43, pp. 591-607, 2007.

[19] D. Deng, "FEM prediction of welding residual stress and distortion in carbon steel considering phase transformation effects," *Materials and Design,* vol. 30, pp. 359-365, 2009.

[20] B. Ali, M.-Z. Marjan, C. Ahmad and J. Mohammad, "Finite element modeling of the electron beam welding of Inconel-713LC gas turbine blades," *Journal of Manufacturing Processes,* vol. 26, 2017.

[21] Livermore Software Technology (LST), *LS-Dyna Keyword User Manual,* 2021.

[22] K. Bzowski, Ł. Rauch, M. Pietrzyk, M. Kwiecie ´n and K. Muszka, "Numerical Modeling of Phase Transformations in Dual-Phase Steels Using Level Set and SSRVE Approaches," *Materials ,* no. 14, p. 5363, 2021.

[23] J. Kohout, "Simple and Precise Description of the Transformation Kinetics," *Materials,* vol. 14, no. 1781, 2021.

[24] P. Tossings and P. Duysinx, "Unconstrained Optimisation- Gradient Methods," in *Structural and multidisciplinary Optimization*, Liège, Course notes, 2020-2021, pp. 54-110.

[25] TRANSMETRA, "Table Of Emissivity Of Various Surfaces," Transmetra, [Online]. Available: www.transmetra.ch. [Accessed 5 June 2023].

[26] V. Terrapon and P. Dewallef, "Free Convection," in *MECA0445 - Heat Transfer*, Course notes, 2020.

[27] G. Rakesh, M. El-Zein and E. Johnson, "A Model Equation for the Convection Coefficient for Thermal Analysis of Welded Structures," in *Trends in Welding Research, Proceedings of the 8th International*, Pine Mountain, USA, 2008.

[28] GmbH DYNAmore, "Implicit: Checlist," 2015. [Online]. Available: https://www.dynasupport.com/howtos/implicit. [Accessed 28 05 2021].

10 Annex

From	To	Austenite	Ferrite	Perlite	Bainite	Martensite	Tempered Martensite	Tempered Bainite
Austenite			990.15	990.15	861.15	701.15		
Ferrite		990.15						
Perlite		990.15						
Bainite		990.15						523.15
Martensite		990.15					473.15	
Base Material		990.15						
Filler/Liquid		1623.15						
T.Martensite		990.15						
T.Bainite		990.15						

Table 7: start temperature for transformation phase

From	To	Austenite	Ferrite	Perlite	Bainite	Martensite	Tempered Martensite	Tempered Bainite
Austenite			861.15	861.15	701.15			
Ferrite		1573.15						
Perlite		1573.15						
Bainite		1573.15						990.15
Martensite		1573.15					990.15	
Base Material		1573.15						
Filler/Liquid		1573.15						
T.Martensite		1573.15						
T.Bainite		1573.15						

Table 8: end temperature for phase transition

From	To	Austenite	Ferrite	Perlite	Bainite	Martensite	Tempered Martensite	Tempered Bainite

Austenite	0.0203522
Ferrite	
Perlite	
Bainite	
Martensite	
Base Material	
Filler/Liquid	0.2
T.Martensite	
T.Bainite	

Table 9 : KM coefficient parameter

From	To	Austenite	Ferrite	Perlite	Bainite	Martensite	Tempered Martensite	Tempered Bainite
Austenite			1	1	1			
Ferrite		1						
Perlite		1						
Bainite		1						
Martensite		1						
Base Material		1						
Filler/Liquid								
T.Martensite		1						
T.Bainite		1						

Table 10: exponent parameter evolution with T (constant all along t)

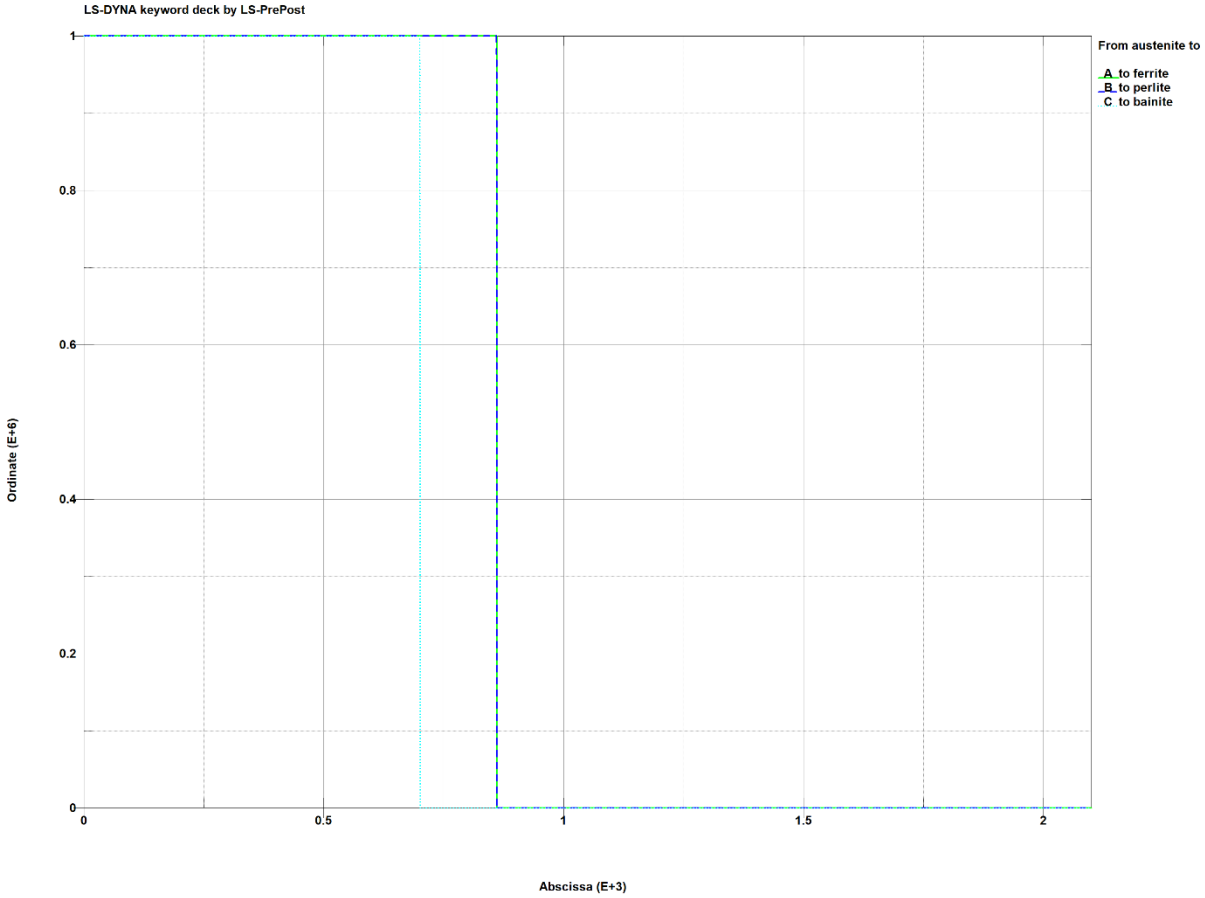

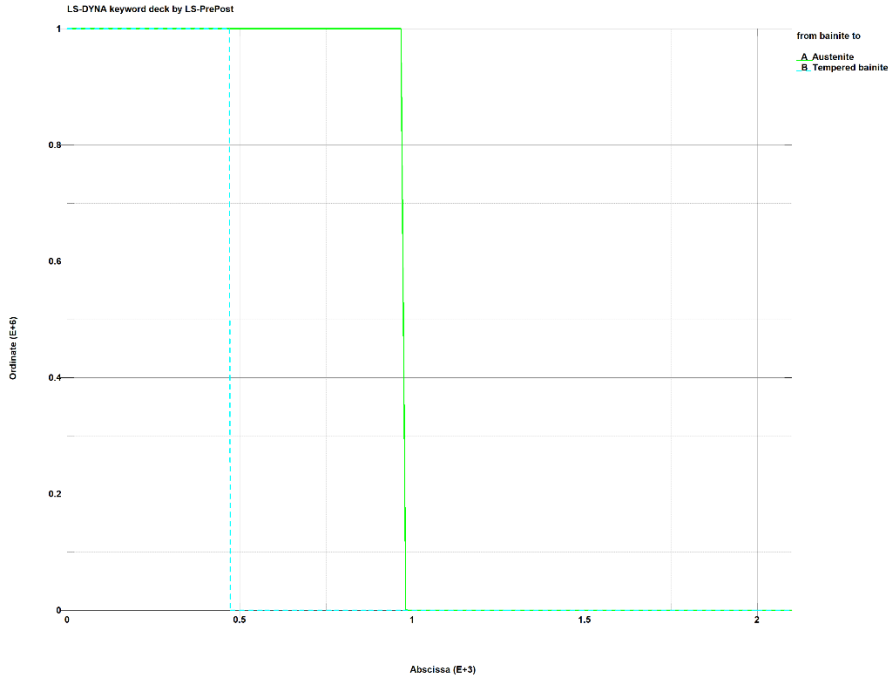

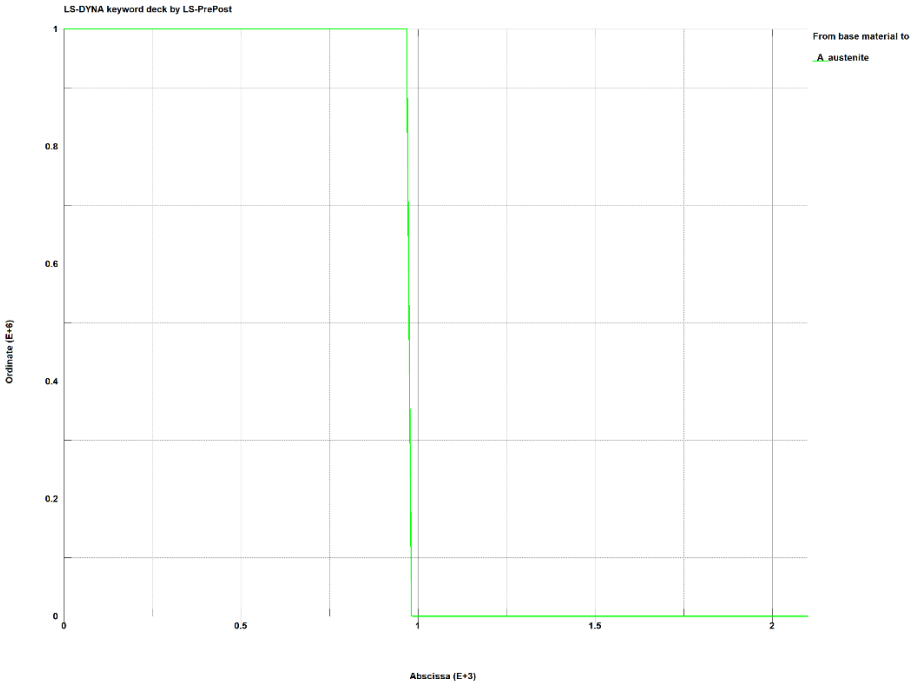

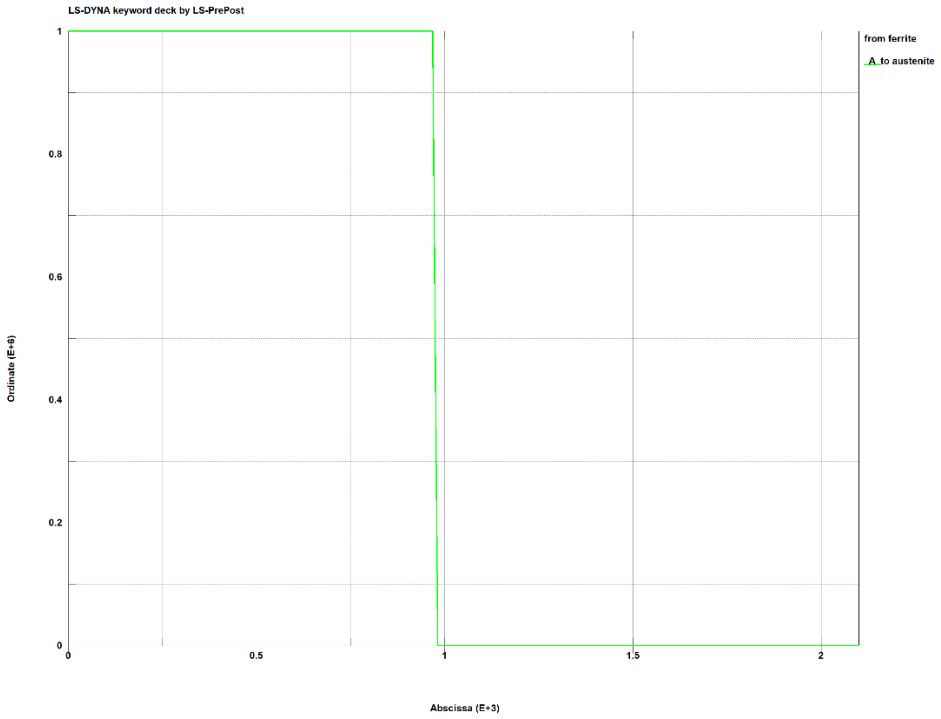

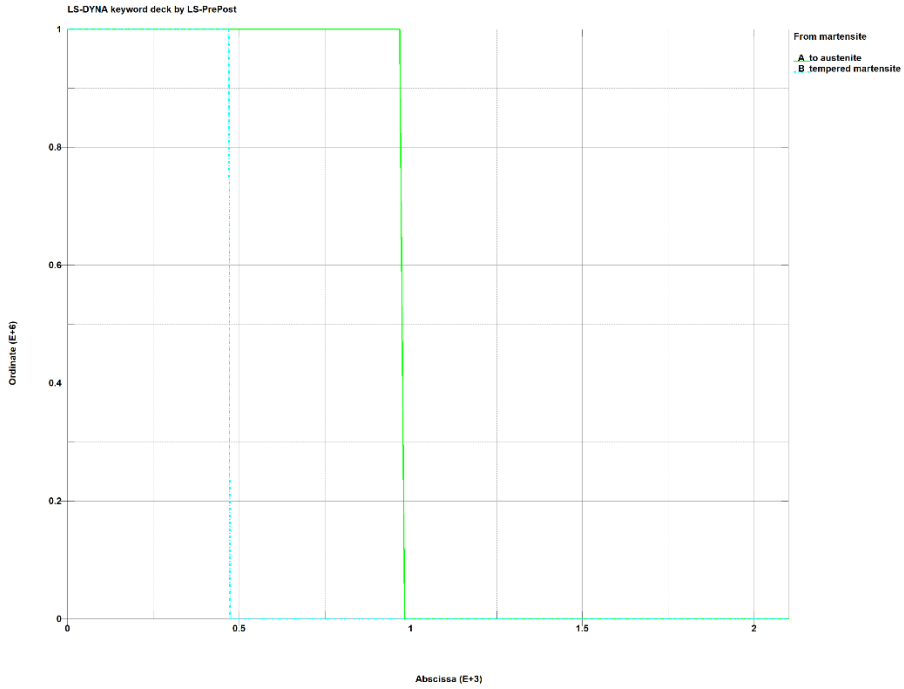

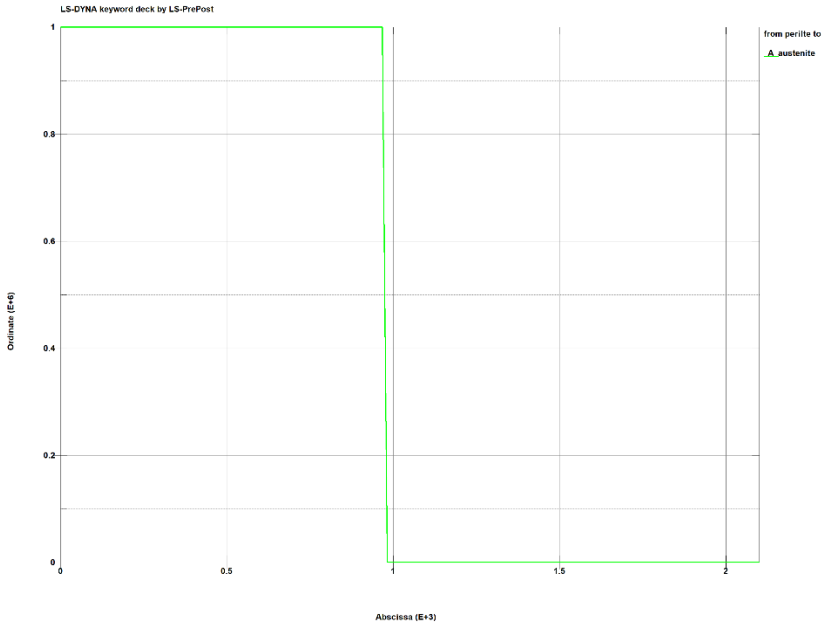

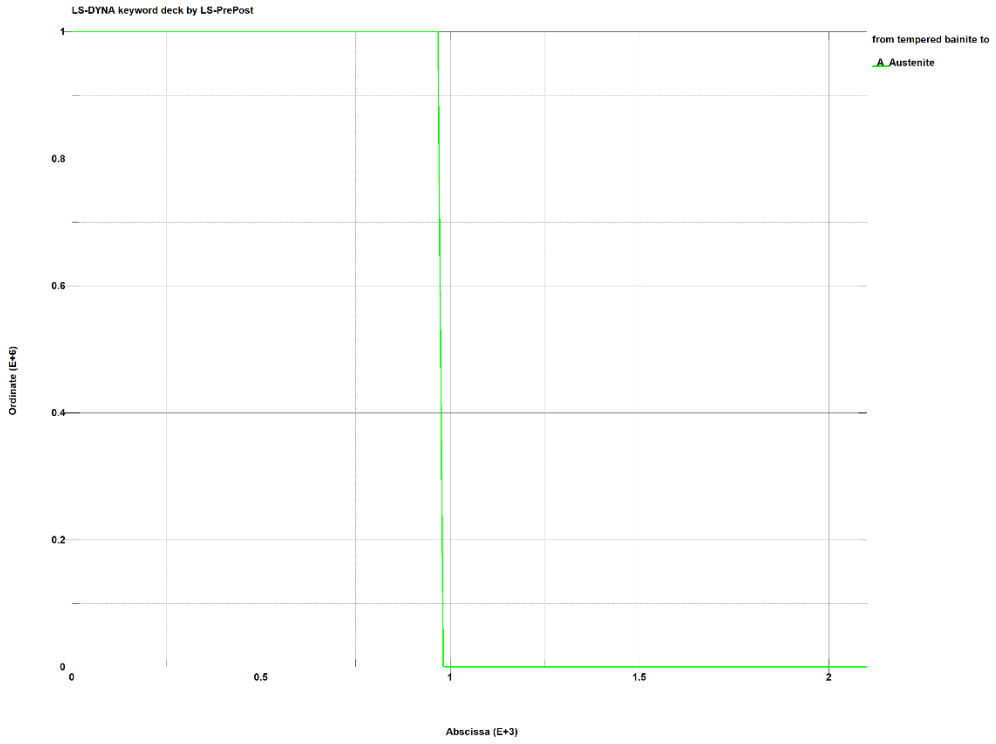

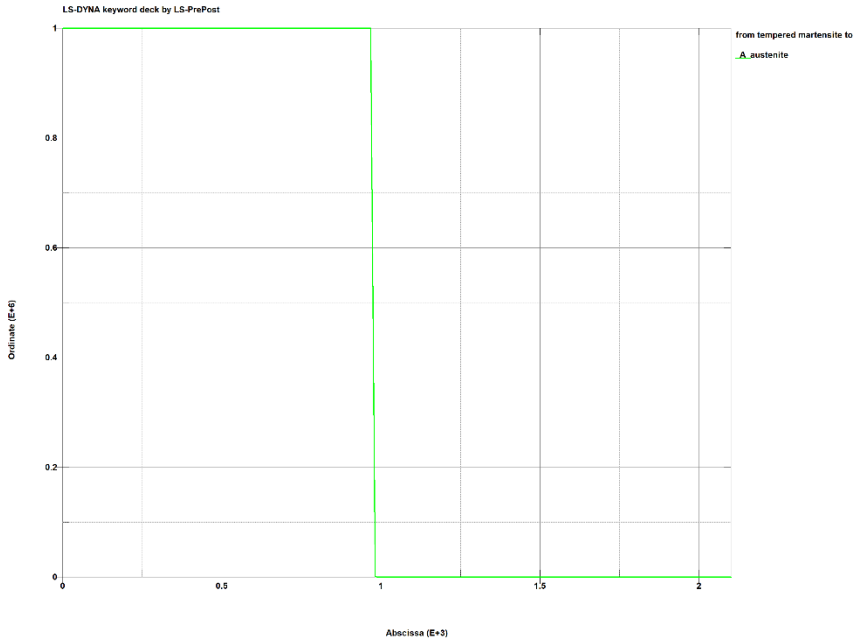

Figure 10-a: tau parameter from JMAK

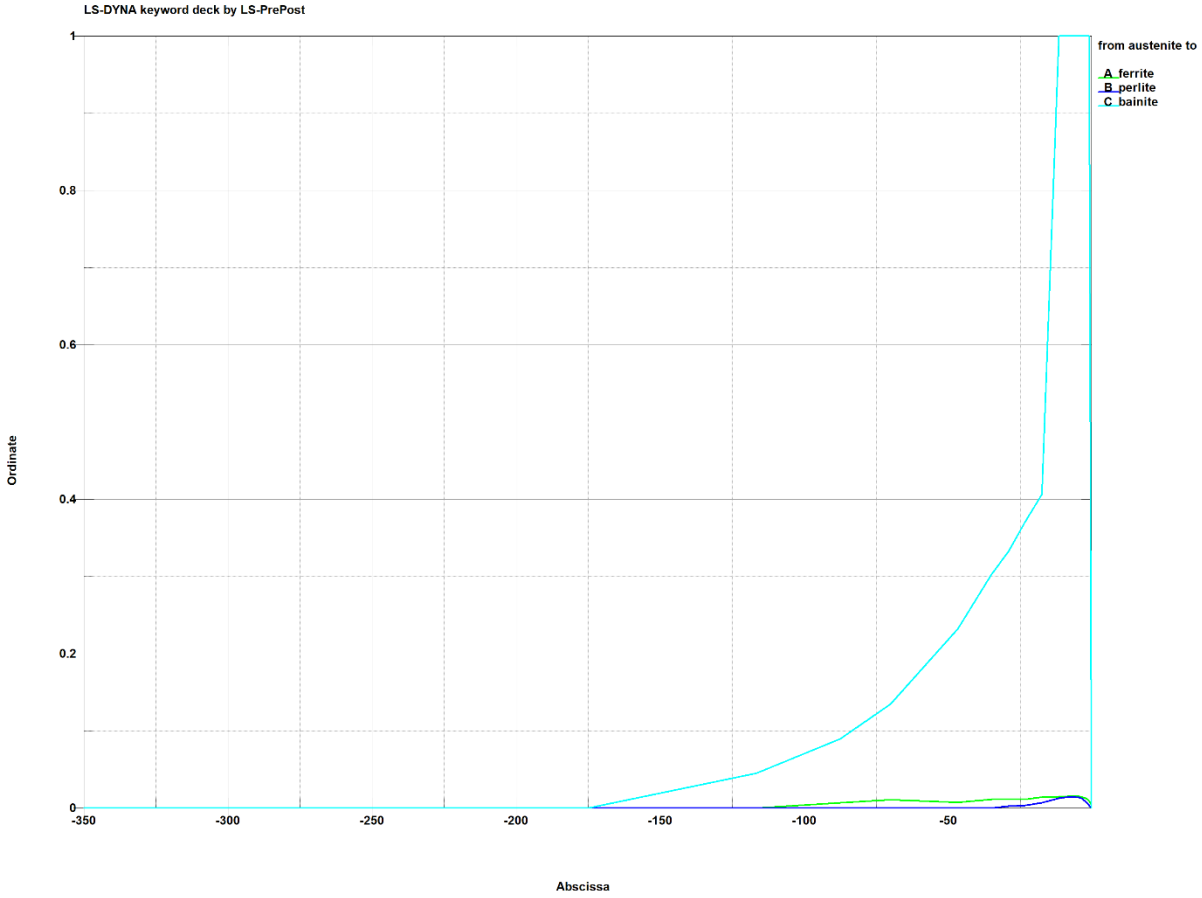

Figure 10-b: Parameter f from JMAK (all other values are constant of one all along temperature) f' has the same values

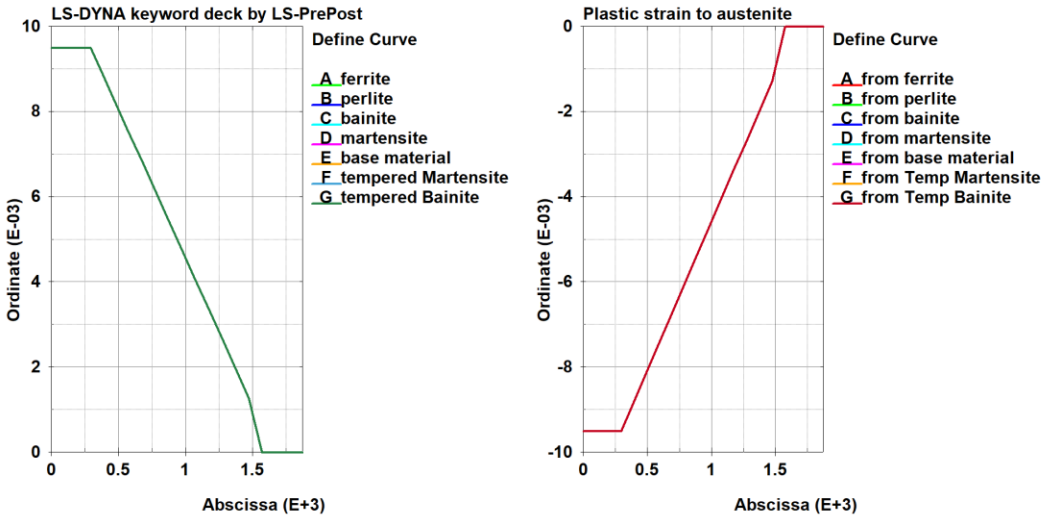

Figure 10-c: PLastic strain from phase transformation, other phase changes are zero

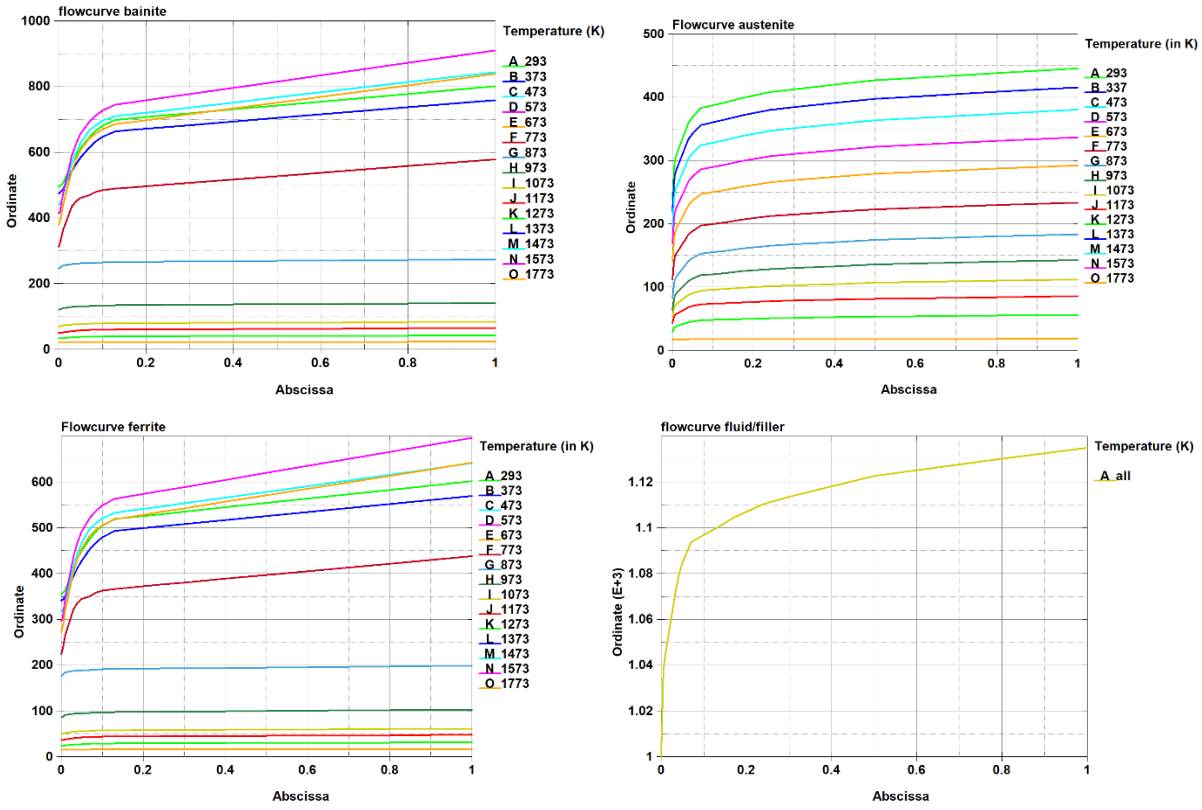

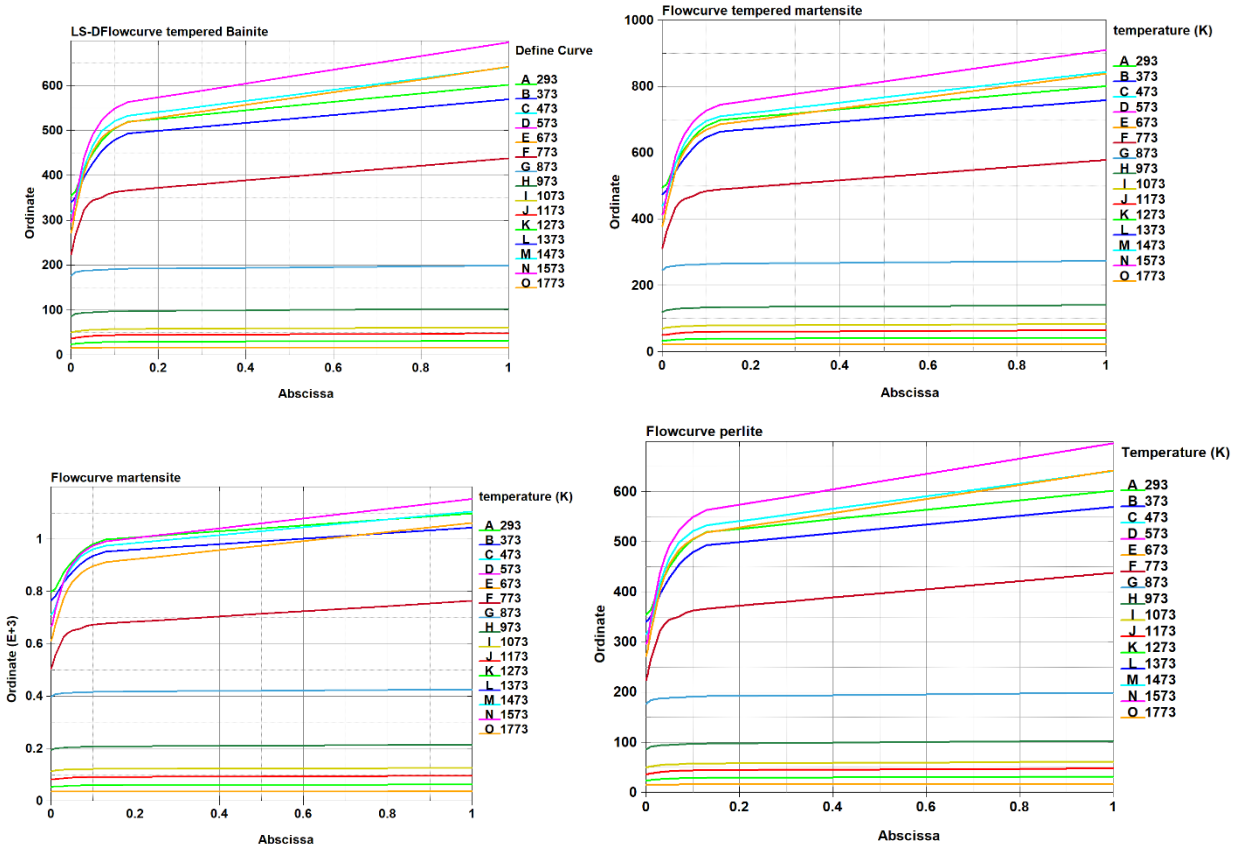

Figure 10-d: flowcurves of the other phases